

Building-up Host-Guest Helicate Motifs and Chains: A Magneto-Structural Study of New Field-Induced Cobalt-Based Single-Ion Magnets

Nathália R. de Campos,^a Cintia A. Simosono,^a Iara M. Landre Rosa,^a Rafaela M. R. da Silva,^a Antônio C. Doriguetto,^a Wallace D. do Pim,^b Tatiana R. Gomes Simões,^c Ana Karoline S. M. Valdo,^d Felipe T. Martins,^d Charlie V. Sarmiento,^e Wallace C. Nunes,^e Guilherme P. Guedes,^f Emerson F. Pedroso,^b Cynthia L. M. Pereira,^g Humberto O. Stumpf,^g Francesc Lloret,^h Miguel Julve,^{h*} and Maria Vanda Marinho.^{a*}

^aInstituto de Química, Universidade Federal de Alfenas, Campus Santa Clara, Alfenas, MG 37133-840, Brazil.

^bDepartamento de Química, Centro Federal de Educação Tecnológica de Minas Gerais, Belo Horizonte, MG 30421-169, Brazil.

^cDepartamento de Química, Universidade Federal do Paraná, Curitiba, PR 81531-980, Brazil.

^dInstituto de Física, Universidade Federal de Goiás, Campus Samambaia, Goiânia, GO 74690-900, Brazil

^eInstituto de Física, Universidade Federal Fluminense, Niterói, Rio de Janeiro, RJ 24210-346, Brazil

^fInstituto de Química, Universidade Federal Fluminense, Niterói, Rio de Janeiro, 24020-141, Brazil.

^gDepartamento de Química-ICEEx, Universidade Federal de Minas Gerais, Belo Horizonte, MG 31270-901, Brazil.

^hDepartament de Química Inorgànica/Institut de Ciència Molecular (ICMol), Universitat de València, C/ catedrático José Beltrán 2, 46980 Paterna, València, Spain.

*Corresponding author: maria.marinho@unifal-mg.edu.br; miguel.julve@uv.es

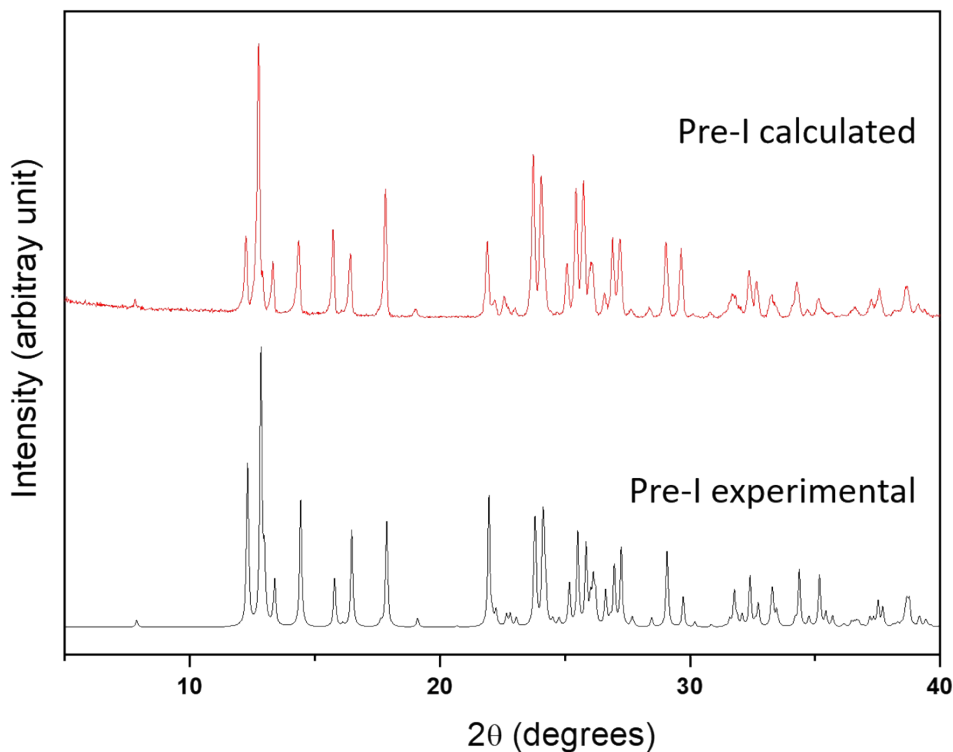


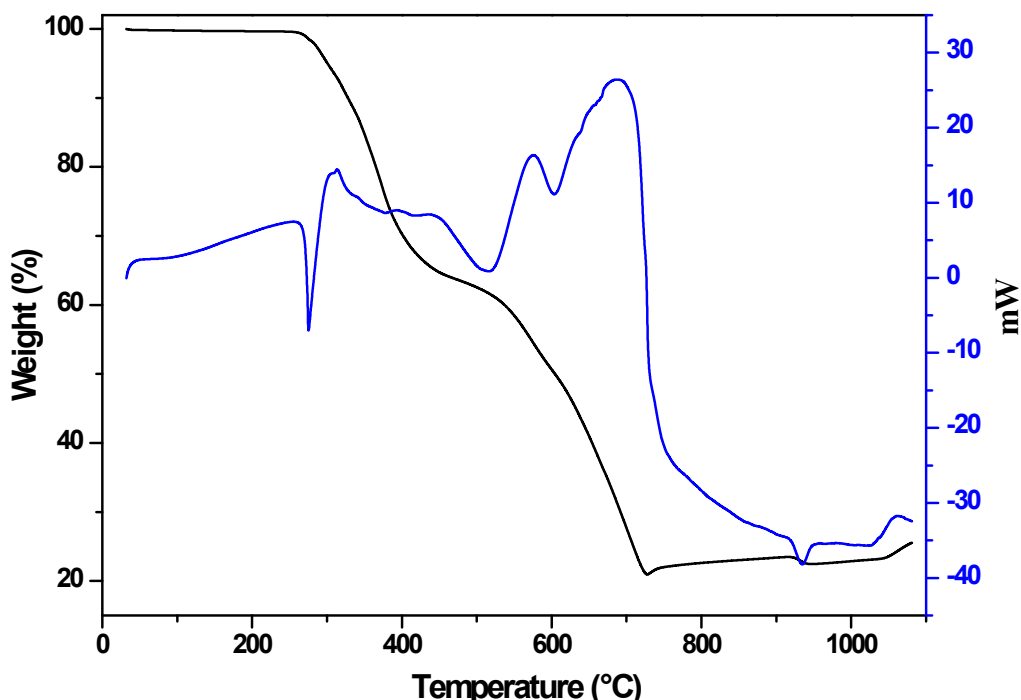
Figure S1 – Experimental and calculated PXRD patterns of **Pre-I**.

*Discussion about TG for **Pre-I** and compounds **I-4**.*

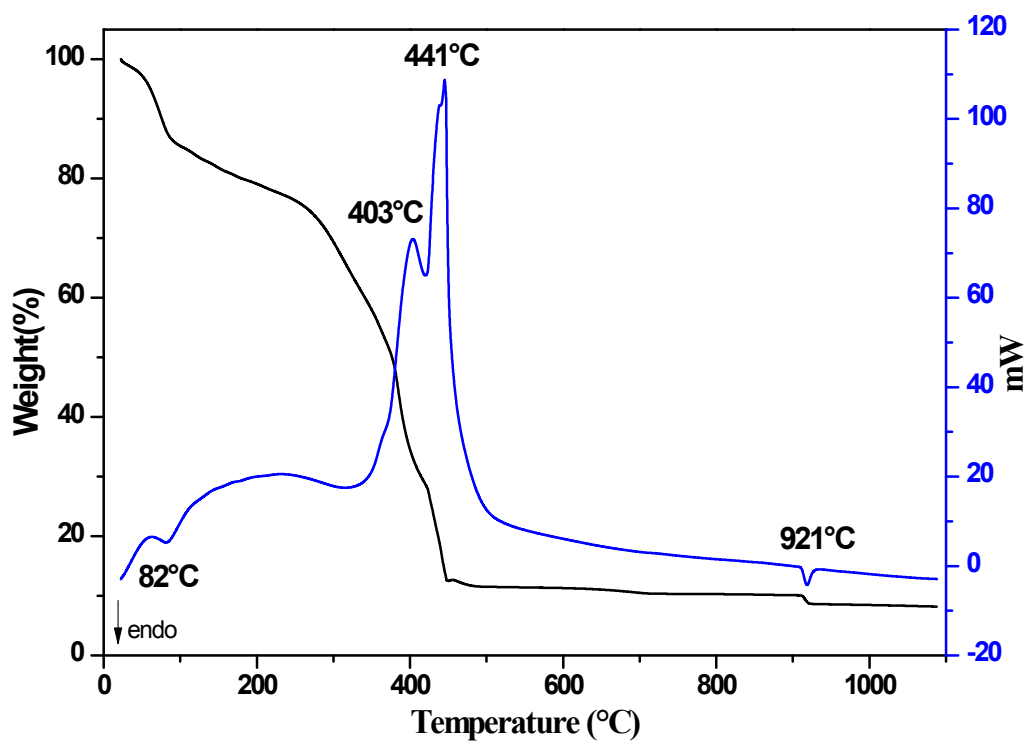
The TG curve of **Pre-I** (Figure S2a) shows that this complex is thermally stable until 270 °C; the DTA curve shows an endothermic peak at 275 °C correspondent to the melting point of **Pre-I**. Then, the decomposition starts with the release of one mol of dpss and one mol of Cl₂ (exp./calc. 79.89/76.88%) probed by two endothermic peaks at 515 and 605 °C. The total weight loss up to 717 °C agrees with the formation of one third of Co₃O₄ (exp./calc. 22.3/22.9%). The last weight loss that occurs between 922 and 944 °C which corresponds to the endothermic peak at 934 °C (DTA), is attributed to the transformation of Co₃O₄ into CoO in agreement with other reduction reactions.¹

The TG curve for **1** exhibits a weight loss of 16.2% (calcd. 16.5%), in an endothermic process centered at 84 °C (onset at 25 °C and ends at 181 °C), which can be attributed to the loss of twelve coordinated water molecules plus one dmso and four water molecules of crystallization. The further weight loss occurring until 468 °C was attributed to the decomposition of organic matter, attributed to six H₂mpba²⁻ units (obsd. 67.1 %; calcd. 67.6 %). The DTA curve shows two exothermic peaks at 403 and 441 °C, due to the thermal decomposition of **1**. The total mass loss up to 468 °C can correspond to 16.7% of the initial mass, and it can be assigned to two Co₃O₄ units (calcd. 21.68%). The last mass loss that occurs between 908 and 932 °C, corresponds to the endothermic peak at 921 °C (DTA) is attributed to the reduction of Co₃O₄ to CoO, as observed for **Pre-I**. The TG curve of **2** shows successive steps, where the first mass loss occurs until 115 °C can be attributed to nine water molecules, nine of them being coordinated and the other three non-coordinated (obsd. 13.2%; calcd. 13.5%), accompanied by DTA curve with an endothermic peak at 115 °C. The subsequent mass loss stages evidence the decomposition step in the temperature range 115-522 °C, which was attributed to two H₂mpba²⁻ units and 0.5 dpss molecules (obsd. 62.2%; calcd. 61.4%), with endothermic (332 °C) and exothermic (378 and 488 °C) processes associated with the decomposition of the ligands. The resulting residue at 907 °C represents 23.0% of the initial mass, which could be related to the formation of Co₃O₄ (calcd. 20.1%), and associated with carbonized material. The reduction of Co₃O₄ to CoO in the TG curve was also observed, accompanied by an endothermic peak at 920 °C (DTA curve). The TG curve for **3** exhibits a first mass loss in the temperature range 25-156 °C, corresponding to the release of four crystallization water molecules (obsd. 9.2%; calcd. 9.4%). The second mass loss between 156 and 422 °C can be assigned to the release of four coordinated water molecules and decomposition of organic matter (1.5 mol H₂mpba) with exothermic processes in the DTA curve at 300, 335, 371, 401 °C

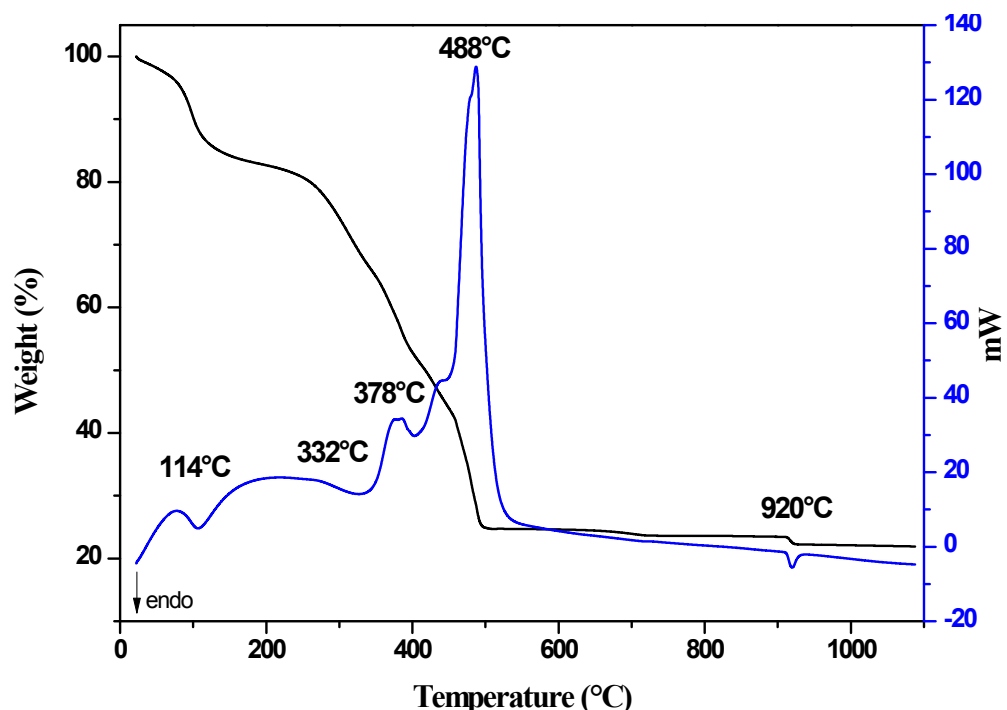
(obsd. 60.4%; calcd. 58.7%), reaching 25.40% of the initial mass as being Co_3O_4 (calcd. 22.62 %) associated to the carbonized material. The reduction of Co_3O_4 to CoO can also be observed at 1034 °C. The TG curve for **4** exhibits a sequence of weight losses between 25 and 197 °C in an endothermic process, with a combined mass loss of 9.3% that would correspond to the release of four coordinated water molecules, one water molecule of crystallization, and four methanol molecules per formula unit (obsd. 9.4%). The further weight loss occurring until 469 °C was attributed to the decomposition of organic matter in four mols of the dpss ligand and thee $\text{H}_2\text{mpba}^{2-}$ ligands (obsd. 67.80%; calcd. 70.4%). This information is corroborated by the DTA curve which shows exothermic peaks at 390 and 463 °C. The final residue corresponding to the 18.96% of the initial mass probably corresponds to four CoO units (obsd. 12.8%) associated with carbonized material from the remaining $\text{H}_2\text{mpba}^{2-}$ ligand. All the TG curves are shown in Figure S2.



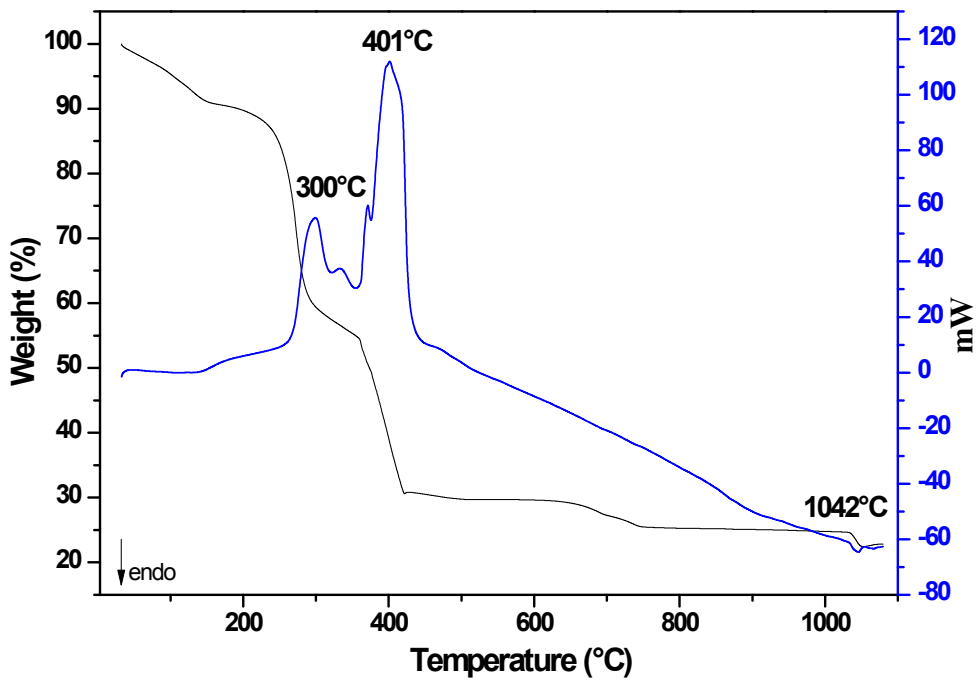
(a)



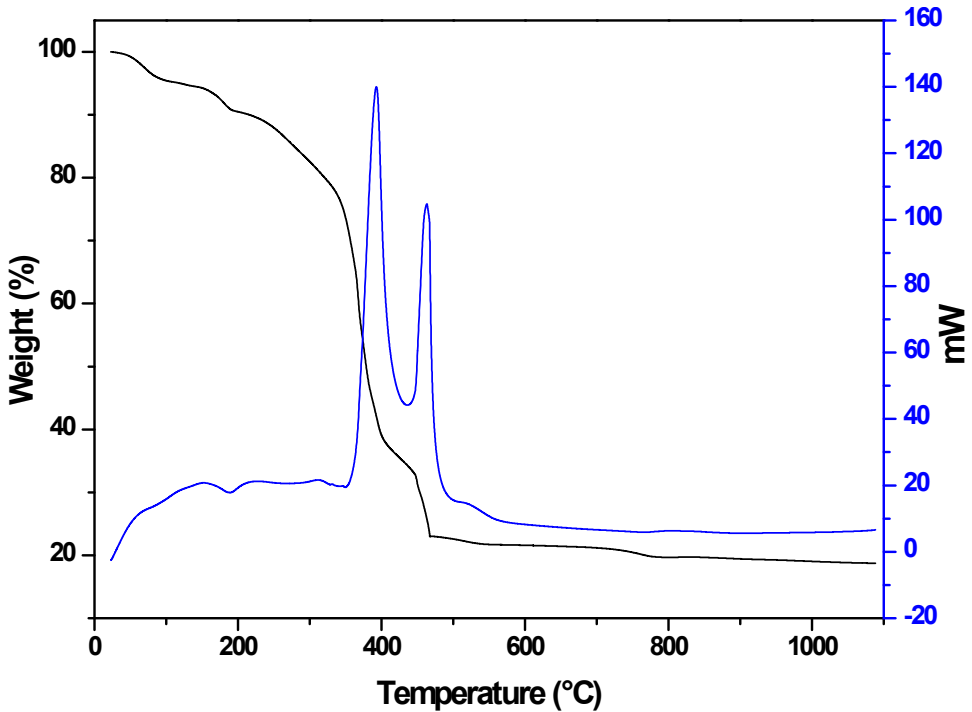
(b)



(c)



(d)



(e)

Figure S2 – TG and DTA curves for (a) Pre-I, (b) 1, (c) 2, (d) 3, and (e) 4.

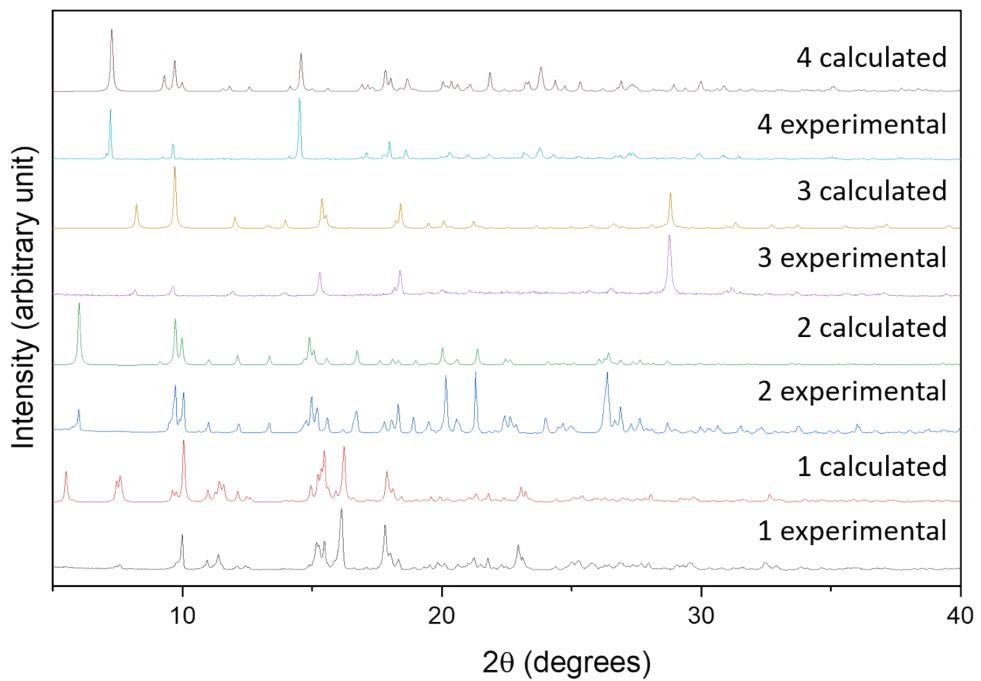


Figure S3 – Experimental and calculated PXRD patterns of **1-4**.

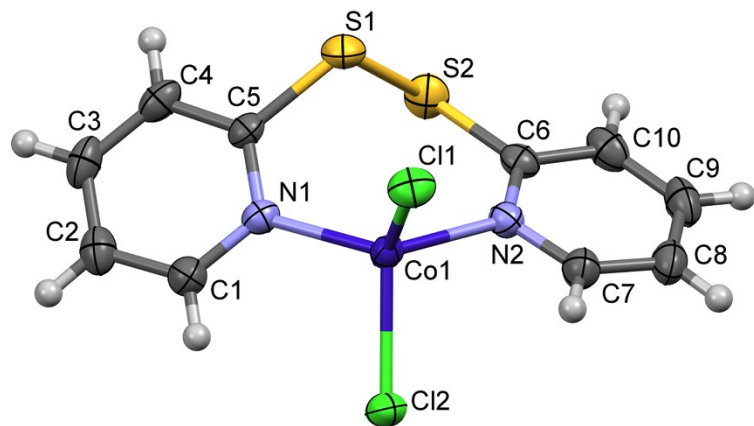


Figure S4– Perspective drawing of the structure of **Pre-I** with the atom labeling. The displacement ellipsoids of the non-hydrogen atoms are drawn at the 50% probability level.

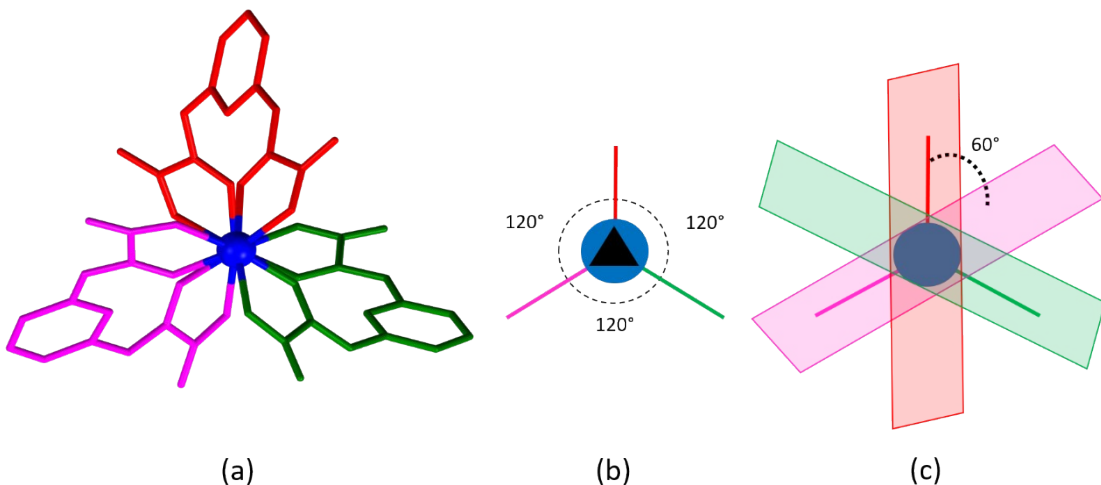
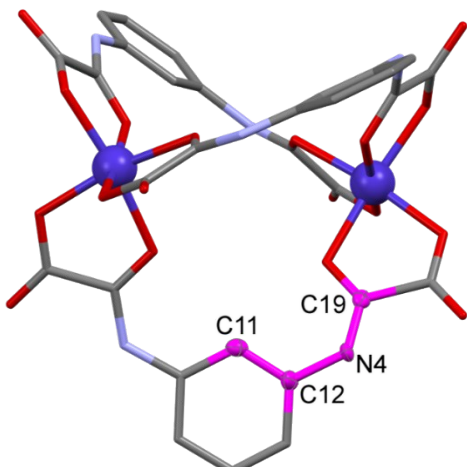
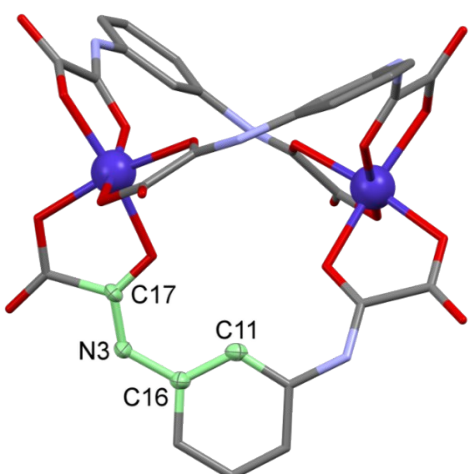


Figure S5 – (a) Mesocate view along the direct crossing of the cobalt(II) ions in **1** and **2**. Simplified representation of the mesocate unit showing (b) the non-crystallographic three-fold rotation axis along the direction crossing the cobalt(II) ions and (c) the 1. s. mean planes calculated for the ligands and the angle of 60° between them.

The least-squares values are 63.22(11), 68.62(13) and 81.43(12) (**1A**), 59.96(10), 76.31(11) and 83.72(11) (**1B**) and 60.76(6), 79.2(19) and 80.9(19)° (**2**). The H₂mpba²⁻ ligands coordinate to the metal ions in a side-by-side arrangement, a feature that imposes a non-planar ligand conformation, as demonstrated by the root-mean-squared deviation (RMSD) for the H₂mpba²⁻ non-hydrogen atoms fitted on the 1. s. plane [0.330, 0.392 and 0.407 (**1A**), 0.382, 0.413 and 0.480 (**1B**) and 0.383 and 0.475 Å (**2**)].



(a)



(b)

Figure S6 – (a) The largest *syn* C–C–N–C torsion of one H₂mpba^{2–} ligand in **1A** mesocate represented in pink. (b) The second *syn* C–C–N–C torsion At the other arm of the same ligand, is represented in green.

The ligands are far from being planar, probably due to the rotation of one of the two N–C bonds connecting the phenyl ring to the oxamate group. In this respect, the largest values of the *syn* C–C–N–C torsion value at one arm of each ligand are –23(2), –33(2) and –39(2) $^{\circ}$ in **1A** (Figure S6a) and 34(2), 39(2) and 41(2) $^{\circ}$ in **1B**. Those at the other arm are –5(2), –17(2) and –22(2) $^{\circ}$ in **1A** (Figure S6b) and 5(2), 12(2) and 14(2) $^{\circ}$ in **1B**. Dealing with the helicate unit in **2**, the values of the *syn* C–C–N–C torsion are 3.6(10) and 38.9(8) $^{\circ}$ for the whole H₂mpba^{2–} ligand in the asymmetric unit and 21.1(10) $^{\circ}$ at both arms of the other oxamate ligand.

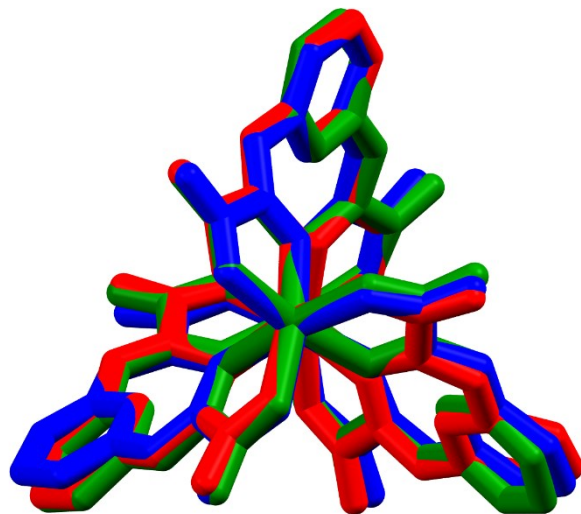


Figure S7– (a) Superposition among the crystallographically independent mesocate units s of the main complex present in **1** (molecules **A** and **B** are colored in blue and green) and **2** (red). A projection normal to the direction crossing through the two cobalt(II) ions from each complex is shown to detach the intramolecular three-fold symmetry axis.

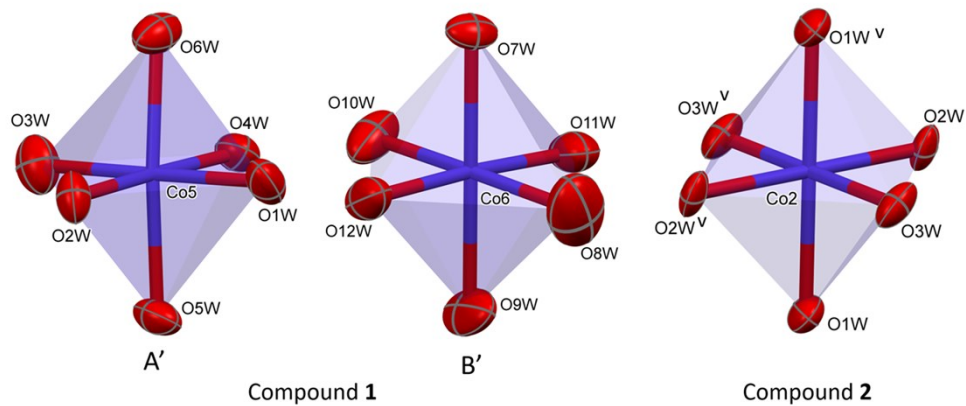


Figure S8 – $[\text{Co}(\text{H}_2\text{O})_6]^{+2}$ counter ions of **1** and **2**, evidencing their octahedral environments. Capital letters (**A'** and **B'**) denote the two crystallographically independent molecules present in the asymmetric unit of **1** [Symmetry code: (v) $1.5-x, -y, 0.5-z$].

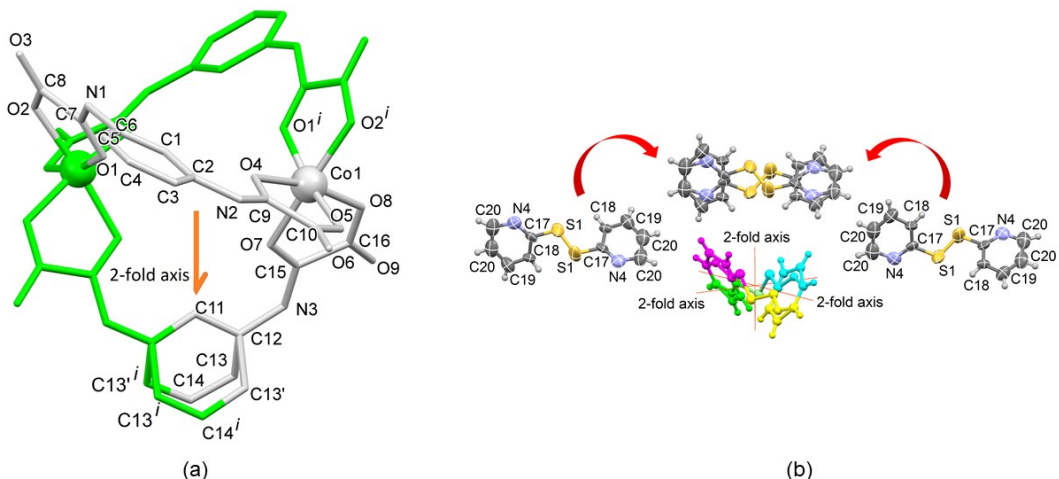


Figure S9— Representation of the crystallographic two-fold rotation axis symmetry and disordered atoms from (a) a helicate unit and (b) the dpss molecule in **2**. A half water molecule is also present in the asymmetric unit, but it was omitted in Figure for the sake of clarity.

The half $[\text{Co}_2(\text{mpba})_3]^{2-}$ helicate found in the asymmetric unit has one cobalt(II) ion, a $\text{H}_2\text{mpba}^{2-}$ ligand and a half of this ligand whose phenylene ring is disordered over two site sets ($\text{C}11$, $\text{C}13$, $\text{C}13'$, and $\text{C}14$ have a site occupancy factor of 0.5, while $\text{C}12$ and the remaining $[\text{Co}_2(\text{mpba})_3]^{2-}$ asymmetric part have full occupancy; Figure S9a). Similarly, two disordered site sets are observed for the dpss molecule after completing its molecular backbone by symmetry ($\text{N}4$, $\text{C}17$, $\text{C}18$, and $\text{C}19$ have a site occupancy factor of 0.5, while $\text{C}20$ has full occupancy because it is the only non-hydrogen atom common to both site sets; Figure S9b).

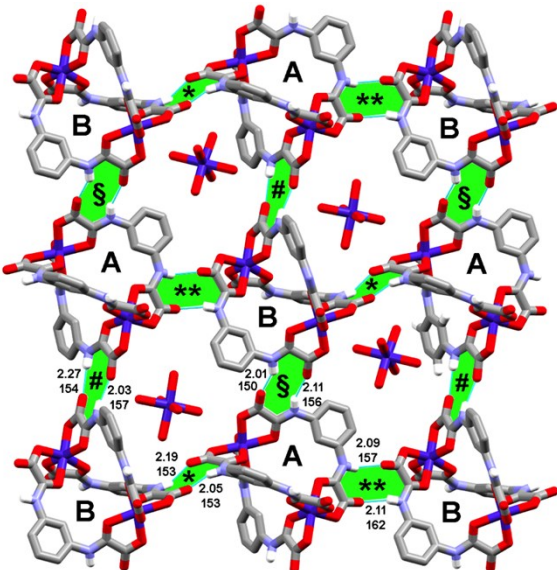


Figure S10– View of the crystal packing of **1** featured by hydrogen-bonded sheets onto the [3¹3] plane through R₂²(10) synthons (shaded in green; equivalent symbols are labeling symmetry-related synthons). Only the hydrogen atoms of the N–H bond are shown. Capital letters refer to the two crystallographically independent helicate units. Hereinafter, hydrogen bonds are pictured as cyan dashed lines and the displayed values refer to the H···A distance (in Å) and D–H···A angle (in deg) [A = acceptor and D = donor].

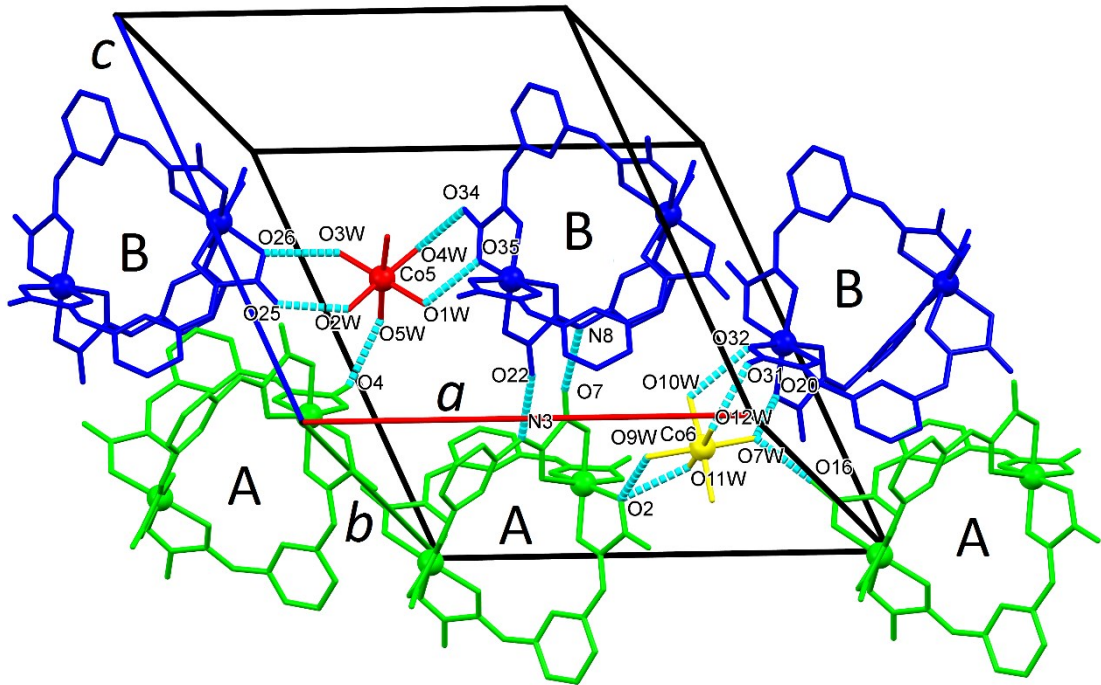


Figure S11 - Packing representation of **1** onto the *ac* plane showing how the layers parallel to [011] plane are cross-connected along the [001] and [100] directions through hydrogen bonds involving the $[\text{Co}(\text{H}_2\text{O})_6]^{+2}$ cations. **A** and **B** mesocates are in green and blue colors, respectively. The two crystallographically-independent $[\text{Co}(\text{H}_2\text{O})_6]^{+2}$ units are depicted in yellow and red, respectively. Hydrogen atoms not involved in the depicted hydrogen bonds were omitted for the sake of clarity. Hydrogen bonds are pictured as cyan dashed lines.

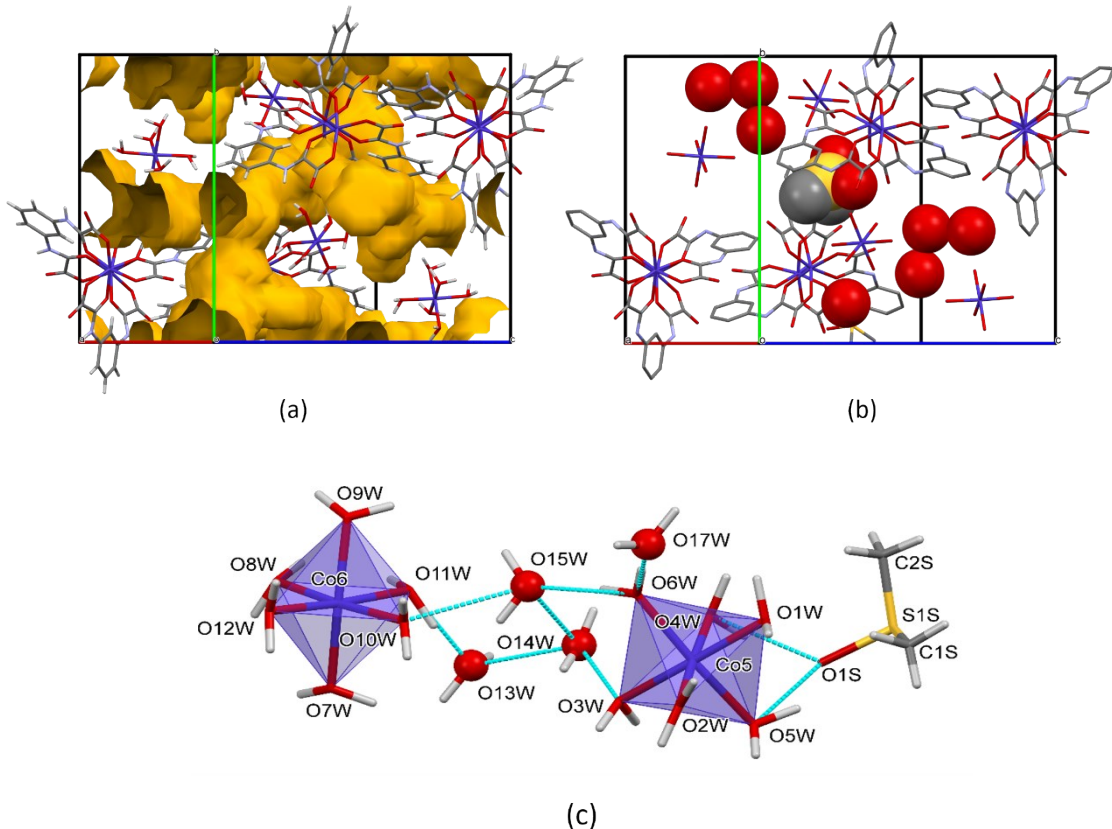
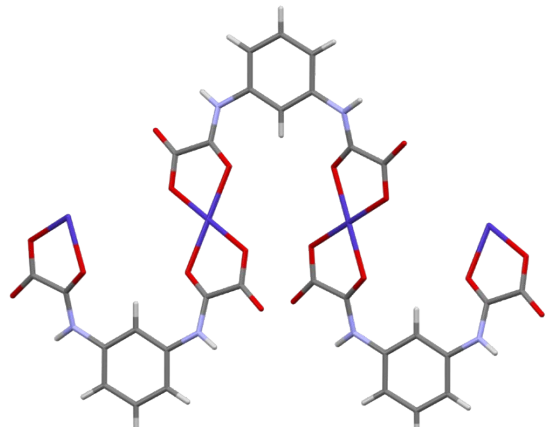
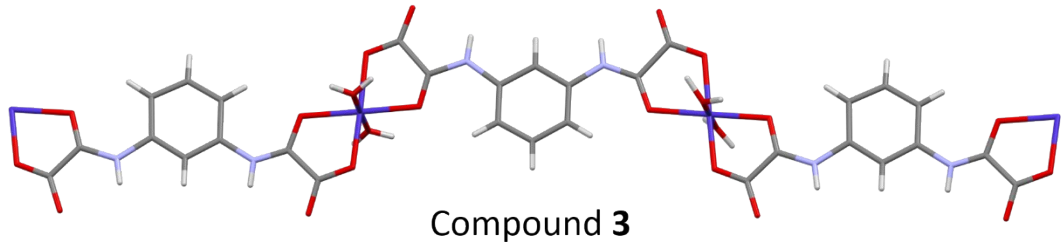
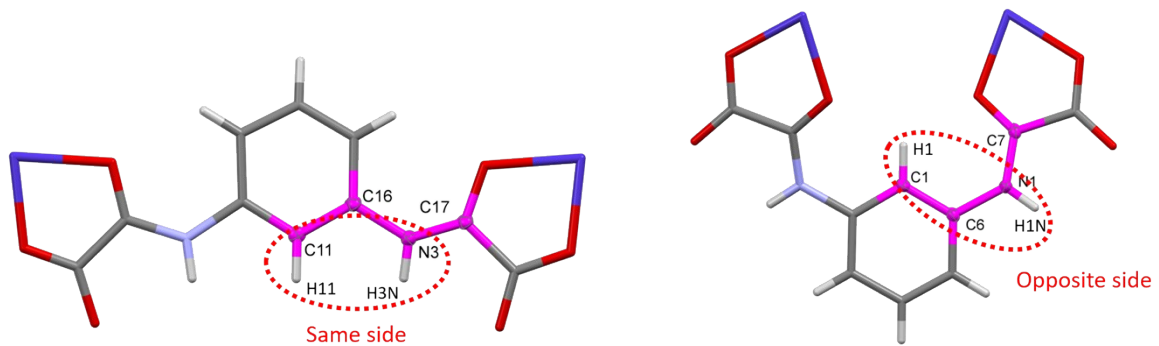


Figure S12 – Packing view of **1** along the b^* axis showing: (a) only the $[\text{Co}_2(\text{H}_2\text{mpba})_3]^{2-}/[\text{Co}(\text{H}_2\text{O})_6]^{2+}$ entities, highlighting the calculated voids (surfaces in orange) across the structure, (b) the whole packing and (c) the hydrogen bonds involving the solvent molecules and hexaaquacobalt(II) units. The voids were calculated by MERCURY using the contact surface approach with a grid spacing and a probing sphere radius of 0.7 and 1.1 Å, respectively. The oxygen atoms of the water molecules were purposely removed from the CIF file before the void calculation.



(a)



Compound **3**

Compound **4**

(b)

Figure S13 – (a) Although **3** and **4** are one-dimensional coordinating polymers, both differ by the linearity of their ligands, since **3** has an almost linear motif while **4** exhibits a snake-shape (water and methanol molecules in **4** were omitted for clarity). (b) Representation of the C-C-N-C torsion for **3** and **4**, highlighting the position of the amide [N3 H3N (**3**) and N1 H1N (**4**)] and the phenyl [C11 H11 for **3** and C1 H1 (**4**)] bonds.

If **1**, **2** and **4** are taken as references, the C–C–N–C torsion in **3** ([177(2) and 178(2) $^{\circ}$ at one ligand and –172(2) and –178(2) $^{\circ}$ at the other one] is equivalent to that of the C11–C12–N4–C19 set of atoms in **1** (Figure S6). Consequently, with regards to oxamate chain, both amide hydrogen atoms are on the same side of that hydrogen atom bonded to the carbon atom at the two position of the phenyl ring (C11 in Figure S13b), while these amide hydrogen atoms are on opposite sides of such C–H hydrogen in **1**, **2**, and **4** (Figure S13b). Thus, the degree of torsion at the N–C phenyl-oxamate bridging bond in **4** [*syn* C–C–N–C = –16.0(5) and –16.9(5) $^{\circ}$] is more similar to the ones found in **1** and **2** than those in **3**. This seems to be related to a higher H₂mpba^{2–} coplanarity in **3** (RMSD of 0.0805 and 0.101 Å for all H₂mpba^{2–} non-hydrogen atoms fitted onto the l. s. plane of each crystallographically independent ligand) with a negligible angle of 0.37(2) $^{\circ}$ between the l. s. planes of the ligands, and in a not so high H₂mpba^{2–} coplanarity in **4** (RMSD of 0.273 Å for all non-hydrogen atoms of the ligand) with the parallel aligned l. s. planes of the ligands risen by 1.53(4) Å. In fact, the torsion at the N–C phenyl-oxamate bridging bond affects the chain conformation as discussed above and it accounts for the different values of the shortest intrachain cobalt-cobalt separation [12.195(6) (**3**) and 5.121(3) Å (**4**)].

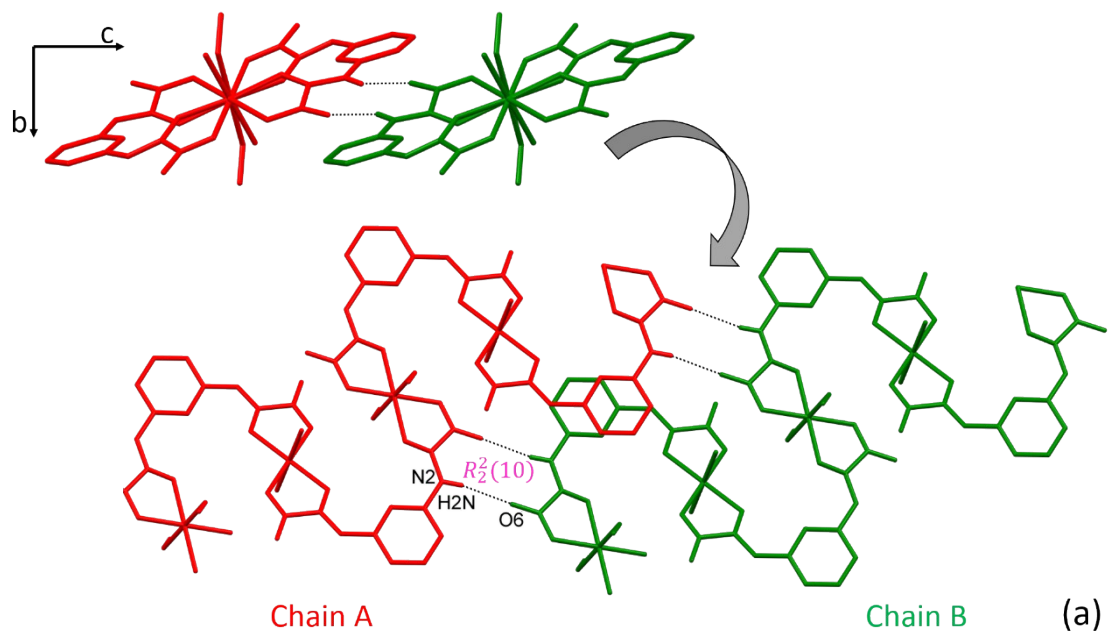


Figure S14— The $R_{2}^{2}(10)$ motifs in **4** occur between the chains along the crystallographic c axis. The hydrogen atoms attached to the carbon ones are hidden for clarity.

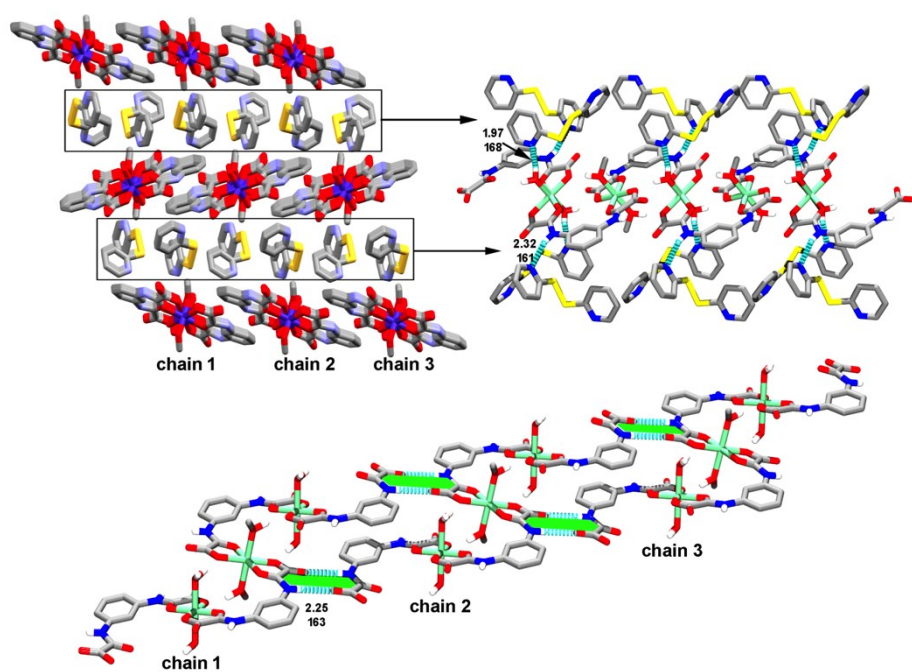


Figure 15– (Top left panel) A packing overview of **4** onto the (100) plane (the free water molecules were omitted for clarity). (Top right panel) A view illustrating the way the

coordinated water molecules and the N–H amide fragment act as hydrogen bond donors towards co-crystallized dpss molecules cross-linking the alternate layers. (Bottom panel) A view of the interlink of the neutral chains along the crystallographic *c* axis through the R₂²(10) motifs (depicted in green). The hydrogen atoms attached to the carbon atoms were omitted for clarity in all panels.

Although each H₂mpba²⁻ ligand has two N–H amide groups to participate in the R₂²(10) hydrogen bonding, only one of them is effective. This is because one N–H group act as hydrogen bonding donor towards one nitrogen atom of free dpss molecule, which in turn, connects a subsequent chain of **4** through a hydrogen bond using its second nitrogen atom, this time acting as an acceptor of the coordinated water molecule. Therefore, the overall packing of **4** can be described as chains running along the [100] direction, which are side-to-side packed through the R₂²(10) motifs along the [001] direction, being these complex entities intercalated by layers of cocrystallized dpss molecules along the [010] direction (Figure S15). This type of interaction (chain-dpss-chain) is repeated infinitely so as to form a supramolecular 3D network.

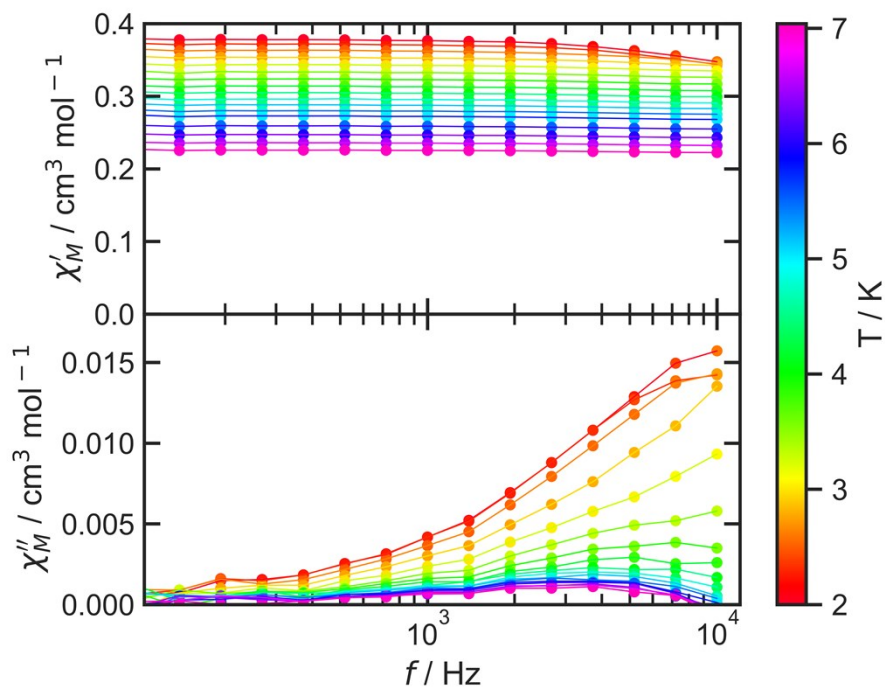


Figure S16– Frequency dependence of the ac susceptibility for **Pre-I**, measured at 1 kOe.
Lines are only eye guides.

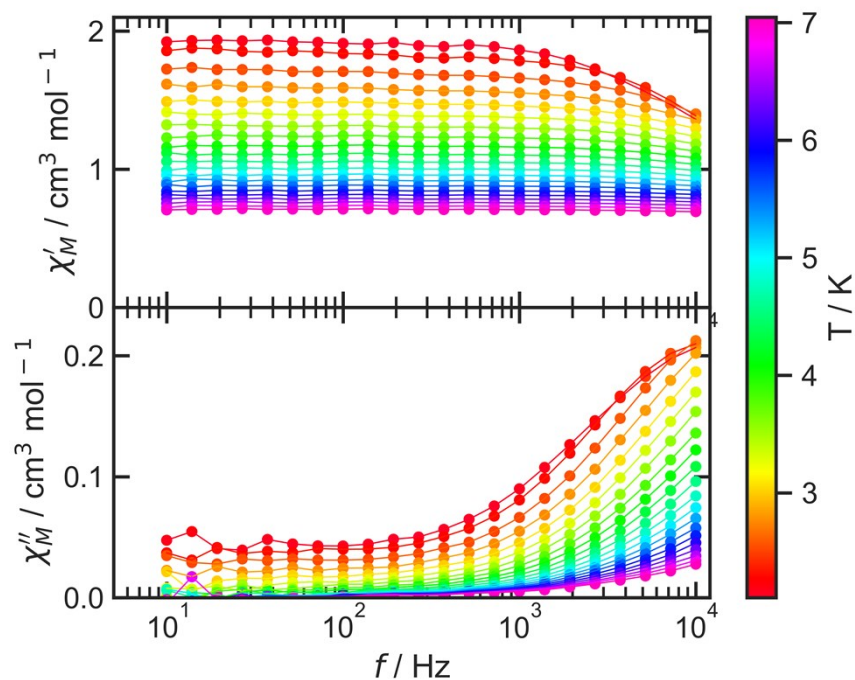


Figure S17– Frequency dependence of the ac susceptibility for **1**, measured at 1 kOe. Lines
are only eye guides.

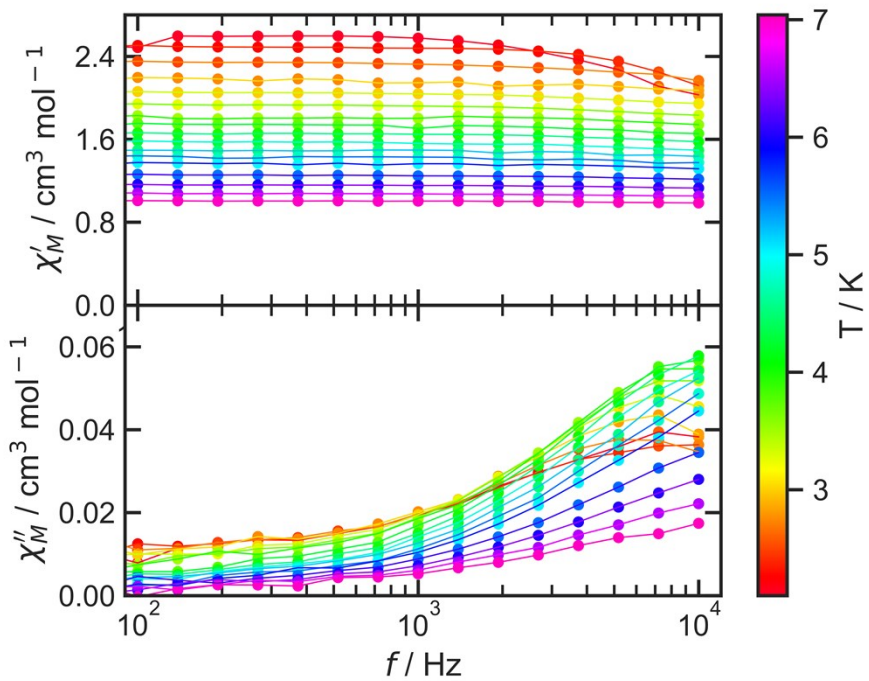


Figure S18– Frequency dependence of the ac susceptibility for **2**, measured at 1 kOe. Lines are only eye guides.

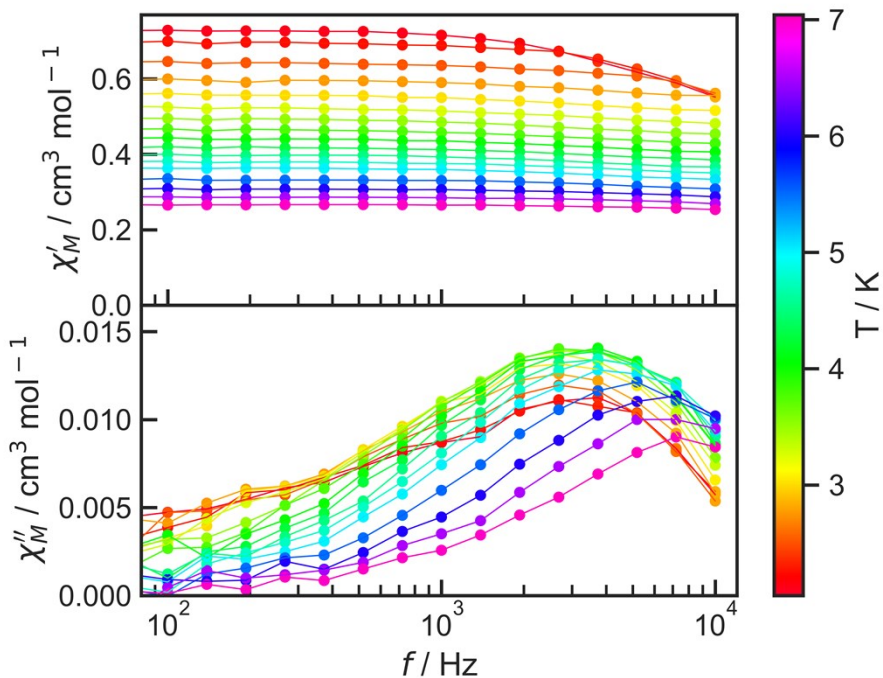


Figure S19– Frequency dependence of the ac susceptibility for **4**, measured at 1 kOe. Lines are only eye guides.

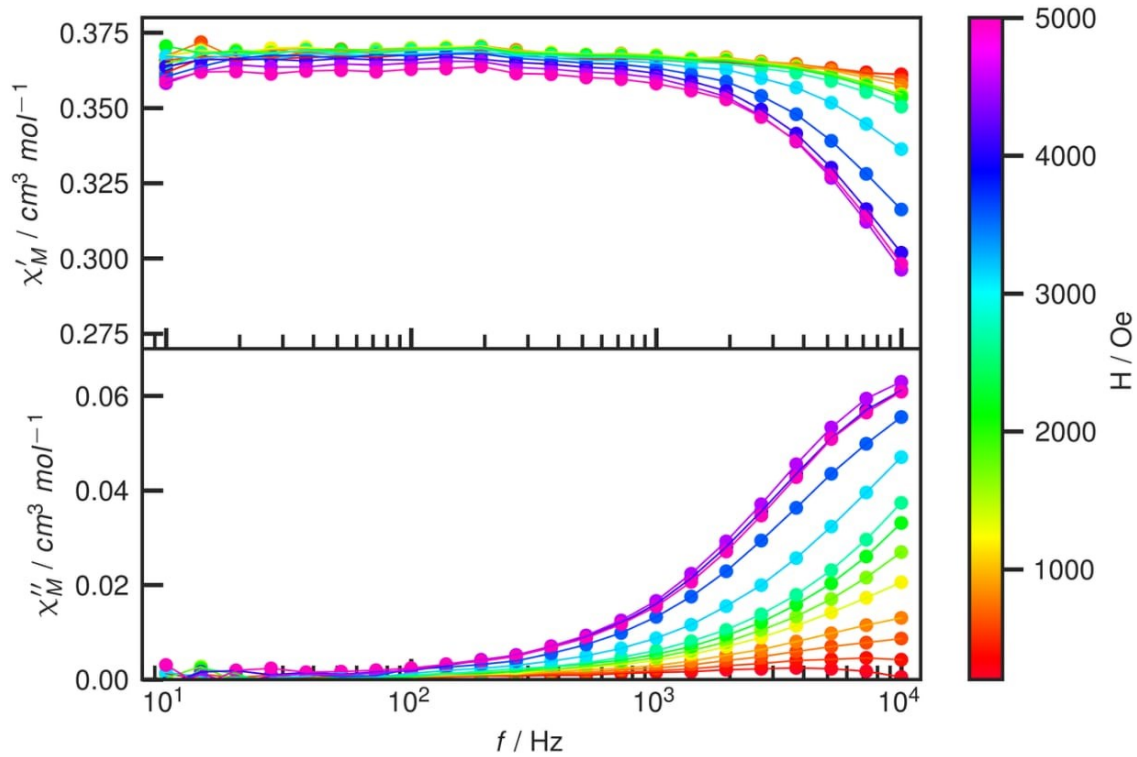


Figure S20- Frequency dependence of the ac susceptibility for **Pre-I**, measured at 2.7 K. Lines are only eye guides.

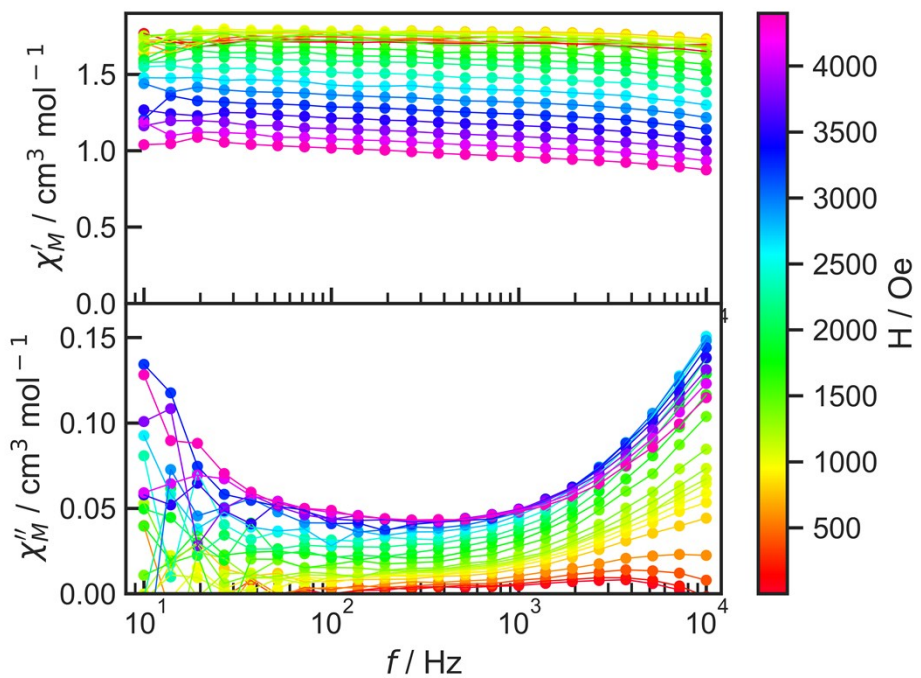


Figure S21- Frequency dependence of the ac susceptibility for **1**, measured at 2.7 K. Lines are only eye guides.

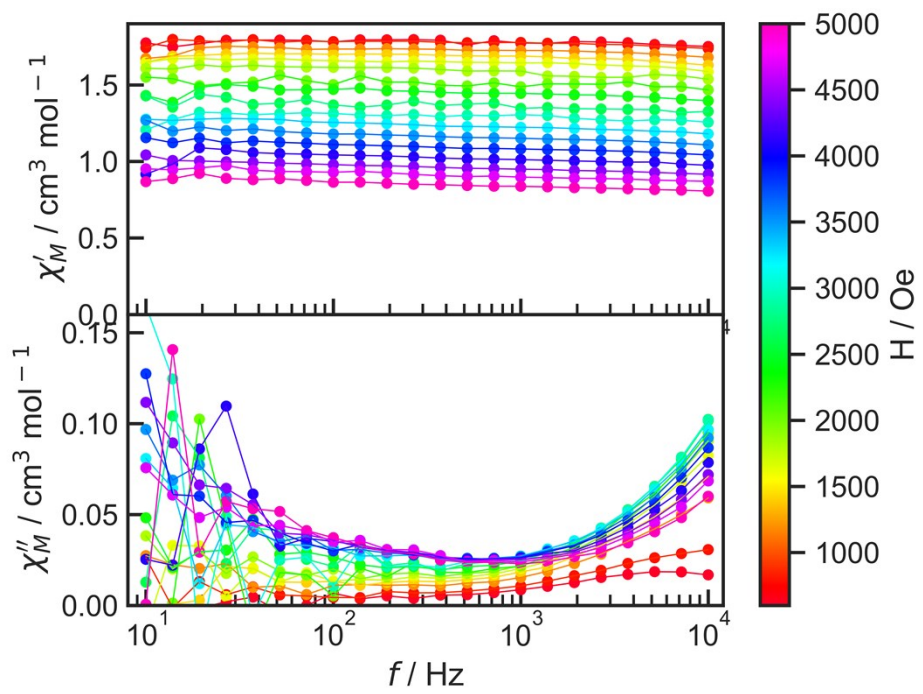


Figure S22- Frequency dependence of the ac susceptibility for **2**, measured at 2.7 K. Lines are only eye guides.

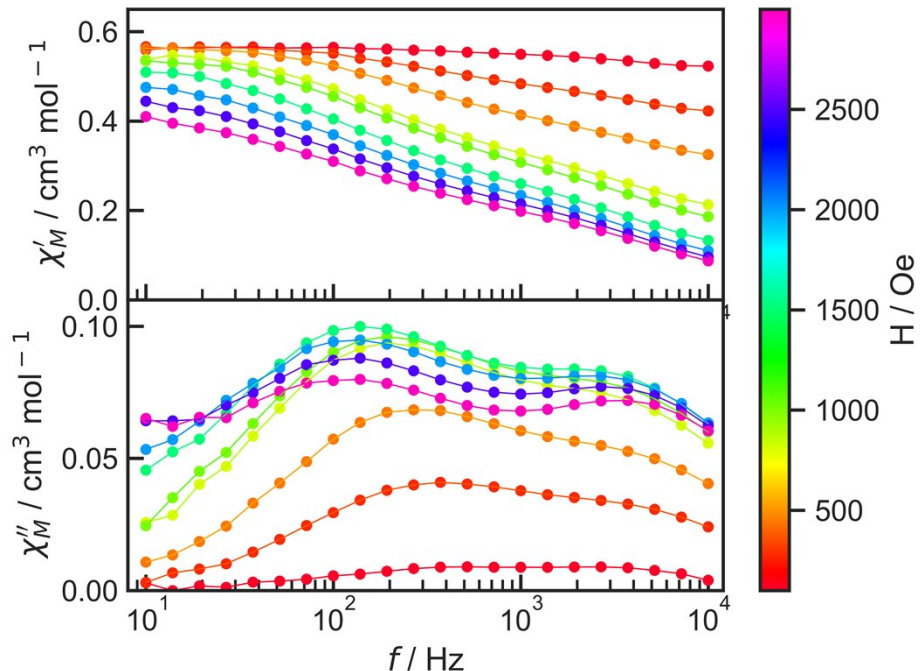


Figure S23– Frequency dependence of the ac susceptibility for **3**, measured at 2.7 K. Lines are only eye guides.

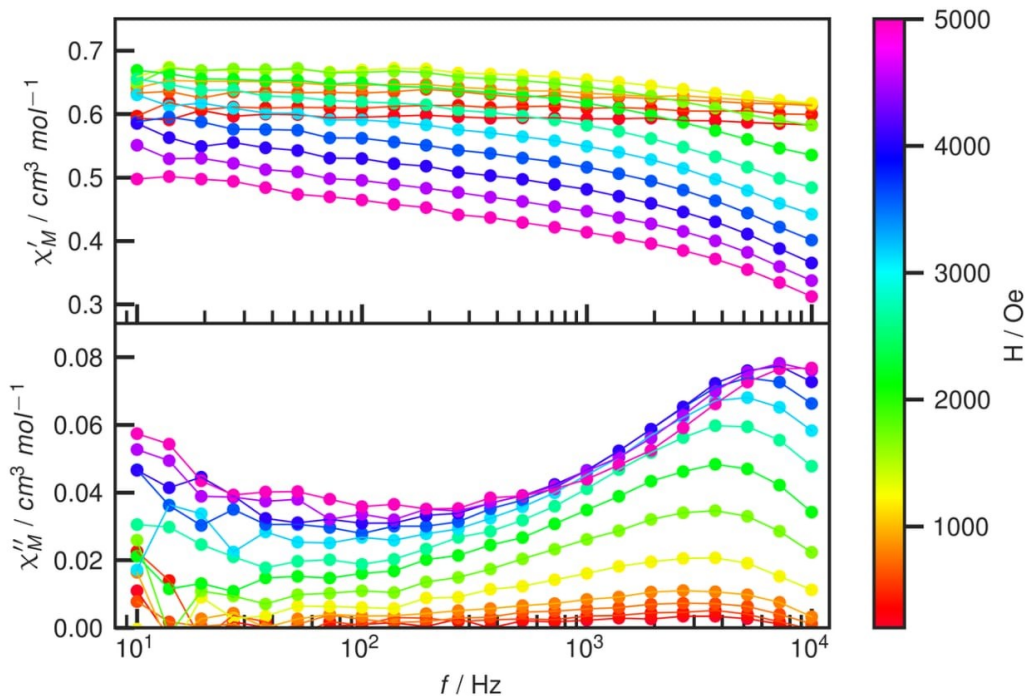


Figure S24– Frequency dependence of the ac susceptibility for **4**, measured at 2.7 K. Lines are only eye guides.

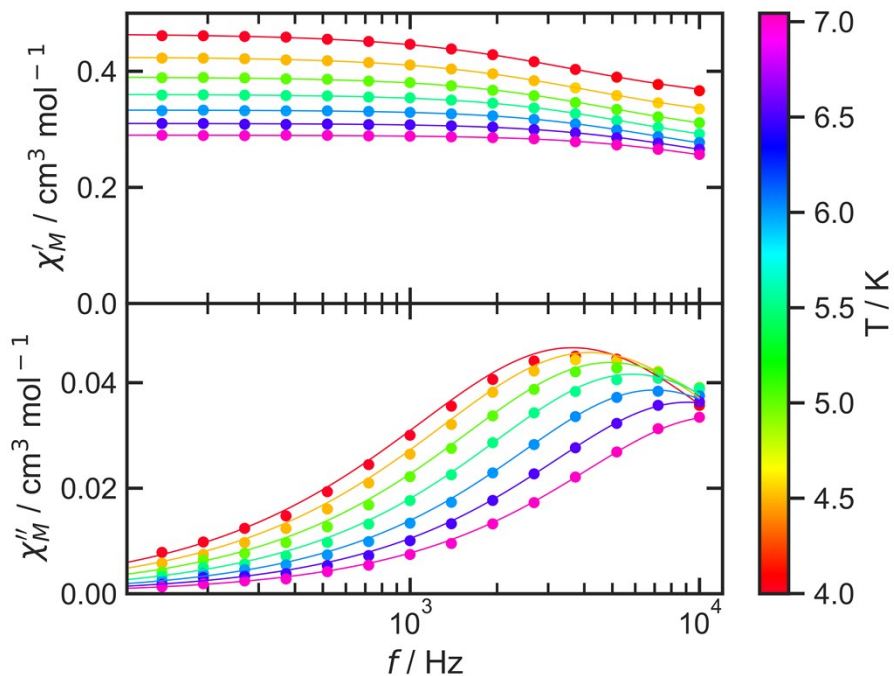


Figure S25– Frequency dependence of the ac susceptibility for **4**, measured at 2 kOe. Lines represent the best-fit curves obtained using a generalized Debye model with one relaxation process according to the description in the text.

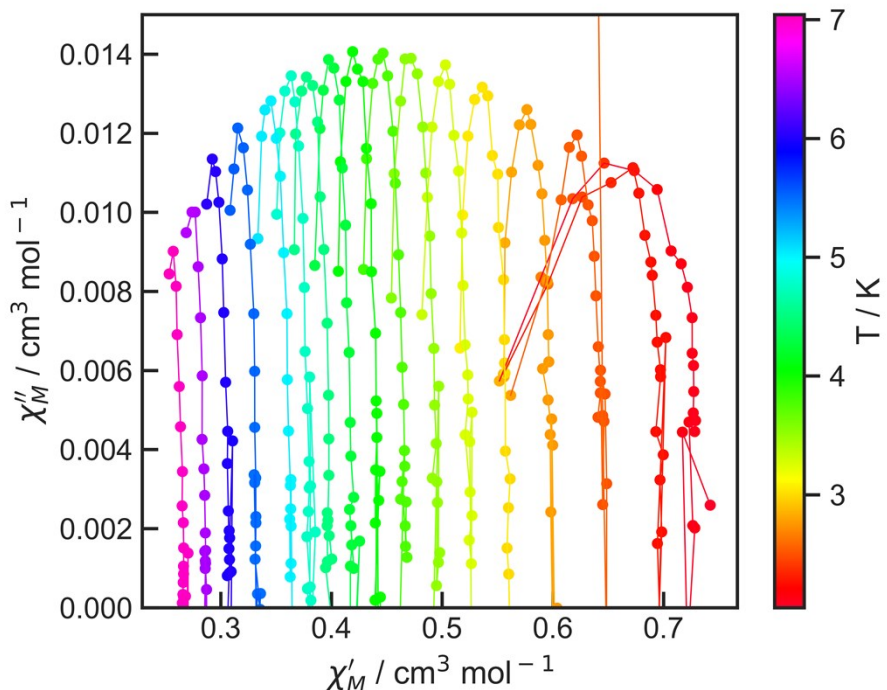


Figure S26– Cole-Cole plot obtained from the frequency-dependence of the ac susceptibility for **4** measured at 1 kOe. Lines are only eye guides.

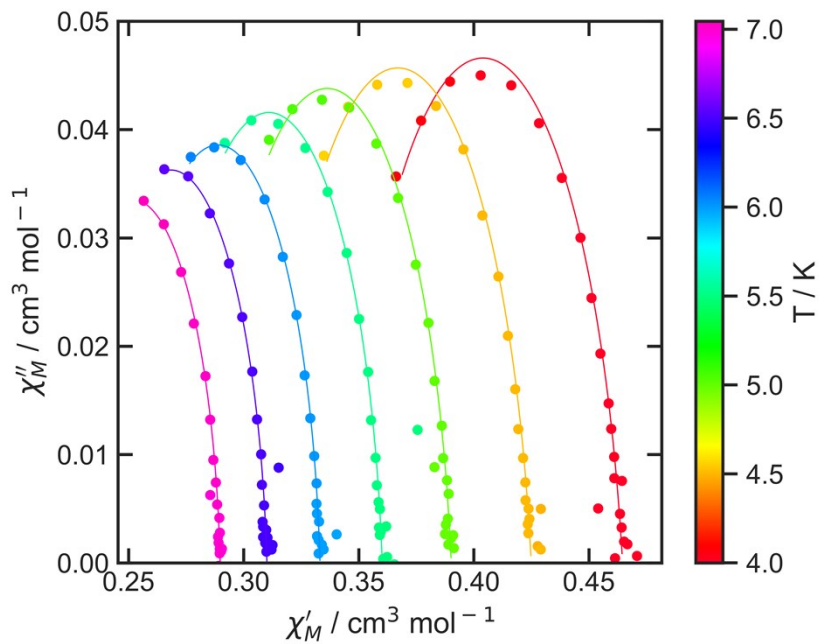


Figure S27– Cole-Cole plot obtained from frequency-dependence of the ac susceptibility for **4** measured at 2 kOe, where the lines represent the obtained fits through a generalized Debye model with one relaxation process.

Table S1 – Selected bond length (Å) and angles (deg) for **Pre-I**

Co1—N1	2.028(3)	N1—Co1—Cl1	113.53(7)
Co1—Cl2	2.250(1)	Cl1—Co1—N2	104.59(7)
Co1—N2	2.062(3)	N2—Co1—Cl1	104.59(7)
Co1—Cl1	2.234(1)	Cl2—Co1—N1	101.95(7)
Cl1—Co1—Cl2	118.46(3)	N1—Co1—Cl2	101.95(7)
Cl2—Co1—Cl1	118.46(3)	Cl2—Co1—N2	100.53(7)
Cl1—Co1—N1	113.53(7)	N2—Co1—Cl2	100.53(7)

Table S2– CShM calculations of the coordination environment at the cobalt(II) ion in **Pre-I**^a

Structure	SP-4	T-4	SS-4	vTBPY-4
Pre-I	26.458	0.944	6.555	3.309

^aAbbreviations: SP-4 = Square (D_{4h}); T-4 = Tetrahedron (T_d); SS-4 = Seesaw (C_{2v}); vTBPY-4 = Vacant trigonal bipyramidal (C_{3v}).

Table S3 – Intermolecular C-H···Cl type interactions in **Pre-I** (Å, deg)^{a,b}

D—H···A	d(D—H)	d(H···A)	d(D···A)	< D—H···A
C2-H2···Cl2 ⁱ	0.93	2.89	3.774(3)	160
C8-H8···Cl2 ⁱⁱ	0.93	2.85	3.661(4)	146
C4-H4···Cl1 ⁱⁱⁱ	0.93	2.74	3.635(4)	162

^aD = Donor and A = acceptor. ^bSymmetry code: (i) = -x, -y+1, -z+2; (ii) = -x, -y, -z+1; (iii) = x, y+1, z.

Table S4 – Bond distances (\AA) for the $\text{O}_{\text{oxamate}}\text{—Co—O}_{\text{oxamate}}$ system in **1**

A mesocate	
Co1—O2	2.083(8)
Co1—O3	2.097(7)
Co1—O8	2.061(8)
Co1—O9	2.117(8)
Co1—O14	2.054(9)
Co1—O15	2.098(8)
Co2—O5	2.101(8)
Co2—O6	2.083(8)
Co2—O11	2.044(8)
Co2—O12	2.127(7)
Co2—O17	2.075(9)
Co2—O18	2.127(7)
B mesocate	
Co3—O20	2.104(8)
Co3—O21	2.083(7)
Co3—O26	2.072(7)
Co3—O27	2.131(7)
Co3—O32	2.075(8)
Co3—O33	2.093(7)
Co4—O23	2.066(8)
Co4—O24	2.099(7)
Co4—O29	2.059(8)
Co4—O30	2.107(8)
Co4—O35	2.079(8)
Co4—O36	2.103(7)

Table S5 – Bond angles (deg) for O_{oxamate}—Co—O_{oxamate} system in **1**

A mesocate	
O14—Co1—O8	91.7(3)
O14—Co1—O2	92.0(3)
O8—Co1—O2	93.1(4)
O14—Co1—O3	96.5(3)
O8—Co1—O3	168.6(3)
O2—Co1—O3	78.7(3)
O14—Co1—O15	79.8(3)
O8—Co1—O15	92.5(3)
O2—Co1—O15	170.2(3)
O3—Co1—O15	96.8(3)
O14—Co1—O9	169.6(3)
O8—Co1—O9	78.8(3)
O2—Co1—O9	92.5(3)
O3—Co1—O9	93.6(3)
O15—Co1—O9	96.4(3)
O11—Co2—O17	96.1(3)
O11—Co2—O6	91.2(3)
O17—Co2—O6	171.3(3)
O11—Co2—O5	94.0(3)
O17—Co2—O5	94.9(3)
O6—Co2—O5	79.9(3)
O11—Co2—O18	172.3(3)
O17—Co2—O18	78.2(3)
O6—Co2—O18	94.9(3)
O5—Co2—O18	91.6(3)
O11—Co2—O12	78.9(3)
O17—Co2—O12	93.5(3)
O6—Co2—O12	92.5(3)
O5—Co2—O12	169.5(3)
O18—Co2—O12	96.2(3)
B mesocate	
O26—Co3—O32	94.4(3)
O26—Co3—O21	93.9(3)
O32—Co3—O21	169.9(3)
O26—Co3—O33	170.6(3)
O32—Co3—O33	79.2(3)
O21—Co3—O33	93.3(3)
O26—Co3—O20	100.1(3)
O32—Co3—O20	93.6(3)
O21—Co3—O20	79.2(3)
O33—Co3—O20	87.2(3)
O26—Co3—O27	80.2(3)
O32—Co3—O27	92.7(3)
O21—Co3—O27	94.5(3)
O33—Co3—O27	93.2(3)
O20—Co3—O27	173.7(3)
O29—Co4—O23	94.6(3)
O29—Co4—O35	94.9(3)

O23—Co4—O35	93.1(4)
O29—Co4—O24	169.8(3)
O23—Co4—O24	78.7(3)
O35—Co4—O24	93.1(3)
O29—Co4—O36	95.7(3)
O23—Co4—O36	167.4(3)
O35—Co4—O36	78.9(3)
O24—Co4—O36	92.0(3)
O29—Co4—O30	78.9(3)
O23—Co4—O30	91.5(3)
O35—Co4—O30	172.6(3)
O24—Co4—O30	93.5(3)
O36—Co4—O30	97.5(3)

Table S6 – Bond distances (\AA) for the $\text{O}_{\text{oxamate}}-\text{Co}-\text{O}_{\text{oxamate}}$ system in **2**^a

Co1—O1 ^{iv}	2.088(4)
Co1—O2 ^{iv}	2.086(4)
Co1—O4	2.080(4)
Co1—O5	2.095(4)
Co1—O7	2.132(4)
Co1—O8	2.072(4)

^aSymmetry code: (iv) = $2.25-x, 0.25-y, z$.

Table S7 – Bond angles (deg) for the $\text{O}_{\text{oxamate}}-\text{Co}-\text{O}_{\text{oxamate}}$ system in **2**^a

O8—Co1—O4	168.05(17)
O8—Co1—O2 ^{iv}	94.18(15)
O4—Co1—O2 ^{iv}	94.95(16)
O8—Co1—O1 ^{iv}	90.12(17)
O4—Co1—O1 ^{iv}	99.22(16)
O2 ^{iv} —Co1—O1 ^{iv}	78.69(16)
O8—Co1—O5	93.34(17)
O4—Co1—O5	78.88(16)
O2 ^{iv} —Co1—O5	90.53(17)
O1 ^{iv} —Co1—O5	168.90(17)
O8—Co1—O7	78.01(15)
O4—Co1—O7	93.59(15)
O2 ^{iv} —Co1—O7	170.29(16)
O1 ^{iv} —Co1—O7	95.39(16)
O5—Co1—O7	95.64(17)

^aSymmetry code: (iv) = $2.25-x, 0.25-y, z$.

Table S8– Continuous shape measurement (CShM) results of the coordination environment of the cobalt(II) ions **1-4**^a

Structure	HP-6	PPY-6	OC-6	TPR-6	JPPY-6
1					
Co1	29.549	25.731	1.059	12.849	29.720
Co2	28.432	26.697	0.980	13.815	30.532
Co3	28.224	26.353	0.919	14.036	29.822
Co4	29.177	25.602	1.061	13.045	29.205
Co5	31.117	28.145	0.132	15.389	31.820
Co6	31.726	28.960	0.102	15.808	32.523
2					
Co1	29.133	25.125	1.186	12.993	28.606
Co2	32.418	29.790	0.025	16.543	33.187
3					
Co1	28.239	27.381	0.599	15.288	30.558
Co2	28.678	27.341	0.591	15.298	30.659
4					
Co1	27.641	27.842	0.791	15.679	30.836
Co2	28.217	28.107	0.668	15.817	31.180

^aAbbreviations: HP-6 = Hexagon (D_{6h}); PPY-6 = Pentagonal pyramid (C_{5v}); OC-6 = Octahedron (O_h); TPR-6 = Trigonal prism (D_{3h}); JPPY-6 = Johnson pentagonal pyramid J2 (C_{5v}).

The SHAPE values concerning the octahedral geometry (OC-6) of the cobalt(II) ions of the helicate units are 1.059, 0.980, 0.919 and 1.061 for Co1, Co2, Co3 and Co4 (**1**) and 1.186 for Co1 (**2**) [compared to those for the trigonal prismatic environment (TPR-6) which cover the range 12.849-15.808]. The SHAPE values of 0.599 (Co1) and 0.591 (Co2) in **3** and 0.791 (Co1) and 0.668 (Co2) in **2** for OC-6 symmetry were found [compared to 15.288 (Co1) and 15.298 (Co2) in **3** and 15.679 (Co1) and 15.817 (Co2) in **4** for the TPR-6

symmetry]. In contrast to what occurs in **3**, the two crystallographically independent cobalt(II) ions in **4** (Co1 and Co2) are centrosymmetric.

Table S9 – Bond distances (\AA) for $[\text{Co}(\text{H}_2\text{O})_6]^{2+}$ in **1**

A' unit	
Co5—O1W	2.086(11)
Co5—O2W	2.053(10)
Co5—O3W	2.097(12)
Co5—O4W	2.106(11)
Co5—O5W	2.117(10)
Co5—O6W	2.066(11)
B' unit	
Co6—O7W	2.079(9)
Co6—O8W	2.064(15)
Co6—O9W	2.113(14)
Co6—O10W	2.061(10)
Co6—O11W	2.065(14)
Co6—O12W	2.022(12)

Table S10 – Bond angles (deg) for $[\text{Co}(\text{H}_2\text{O})_6]^{2+}$ in **1**

A' unit	
O2W—Co5—O6W	96.4(5)
O2W—Co5—O1W	87.0(4)
O6W—Co5—O1W	88.4(4)
O2W—Co5—O4W	177.8(4)
O6W—Co5—O4W	84.8(5)
O1W—Co5—O4W	91.1(5)
O2W—Co5—O3W	92.5(4)
O6W—Co5—O3W	91.0(5)
O1W—Co5—O3W	179.2(6)
O4W—Co5—O3W	89.4(5)
O2W—Co5—O5W	88.0(4)
O6W—Co5—O5W	175.3(5)
O1W—Co5—O5W	90.1(5)
O4W—Co5—O5W	90.8(4)
O3W—Co5—O5W	90.5(5)
B' unit	
O12W—Co6—O11W	176.3(5)
O12W—Co6—O10W	91.5(6)
O11W—Co6—O10W	88.0(6)
O12W—Co6—O8W	92.3(7)
O11W—Co6—O8W	88.1(8)
O10W—Co6—O8W	175.4(7)
O12W—Co6—O7W	89.4(5)
O11W—Co6—O7W	94.3(4)
O10W—Co6—O7W	89.2(4)
O8W—Co6—O7W	93.4(7)
O12W—Co6—O9W	91.5(5)
O11W—Co6—O9W	84.8(5)
O10W—Co6—O9W	89.6(6)
O8W—Co6—O9W	87.7(8)
O7W—Co6—O9W	178.5(6)

Table S11 – Bond distances (Å) for $[\text{Co}(\text{H}_2\text{O})_6]^{2+}$ in **2**

Co2—O2W ⁱⁱ	2.049(5)
Co2—O2W	2.049(5)
Co2—O3W ⁱⁱ	2.085(5)
Co2—O3W	2.086(5)
Co2—O1W	2.094(5)
Co2—O1W ⁱⁱ	2.095(5)

[Symmetry code: (ii) = 1.5- x , - y , 0.5- z].

Table S12 – Bond angles (deg) for $[\text{Co}(\text{H}_2\text{O})_6]^{2+}$ in **2**

O2W ⁱⁱ —Co2—O2W	180.0
O2W ⁱⁱ —Co2—O3W ⁱⁱ	91.7(2)
O2W—Co2—O3W ⁱⁱ	88.3(2)
O2W ⁱⁱ —Co2—O3W	88.3(2)
O2W—Co2—O3W	91.7(2)
O3W ⁱⁱ —Co2—O3W	180.0
O2W ⁱⁱ —Co2—O1W	89.6(2)
O2W—Co2—O1W	90.4(2)
O3W ⁱⁱ —Co2—O1W	89.7(2)
O3W—Co2—O1W	90.3(2)
O2W ⁱⁱ —Co2—O1W ⁱⁱ	90.4(2)
O2W—Co2—O1W ⁱⁱ	89.6(2)
O3W ⁱⁱ —Co2—O1W ⁱⁱ	90.3(2)
O3W—Co2—O1W ⁱⁱ	89.7(2)
O1W—Co2—O1W ⁱⁱ	180.0

[Symmetry code: (ii) = 1.5- x , - y , 0.5- z].

Table S13 – Hydrogen bonds in **1** (Å, deg)^{a,b}

	d(D–H)	d(H···A)	d(D···A)	<D···A
O1w–H1A···O35 ^{vi}	0.99	1.76	2.6951(1)	155
O2w–H2b···O25 ^{vii}	0.99	1.79	2.6630(1)	144
N2–H2N···O31 ^{viii}	0.86	2.06	2.8549(1)	153
O3w–H3A···O26 ^{vii}	1.00	2.59	3.5202(1)	155
N3–H3N···O22 ^{ix}	0.86	2.07	2.8861(1)	158
O4w–H4A···O1S ^x	0.99	1.84	2.7812(1)	157
O4w–H4b···O34 ^{xi}	0.99	2.02	2.8886(1)	145
N4–H4N···O19 ^{xi}	0.86	2.12	2.9229(1)	155
O5w–H5A···O4 ^{vii}	0.99	1.89	2.8414(1)	159
O5w–H5b···O1S ^x	1.00	2.18	2.8403(1)	122
N5–H5N···O28 ^{xii}	0.86	2.23	3.0359(1)	156
O6w–H6A···O15w ^{vi}	0.99	1.87	2.8427(1)	164
O6w–H16b···O17w ^{vi}	0.99	1.77	2.7453(1)	166
O7w–H7A···O16 ^{xiii}	1.00	1.79	2.7015(1)	151
O7w–H7b···O20 ^{vii}	1.00	1.90	2.7437(1)	141
N7–H7N···O10 ^{viii}	0.86	2.03	2.8009(1)	149
O8w–H8A···O1 ^{xiv}	0.99	2.39	3.2415(1)	143
N8–H8N···O7 ^{xii}	0.86	2.11	2.9384(1)	161
O9w–H9A···O2 ^{xiv}	0.97	2.11	2.7385(1)	121
O10w–H10b···O32 ^{vii}	0.98	1.97	2.9183(1)	162
N10–H10N···O13 ^{ix}	0.86	2.03	2.8427(1)	156
O11w–H11A···O13w ^{vi}	0.99	1.84	2.6570(1)	139
N11–H11N···O4 ^{xi}	0.86	2.20	2.9869(1)	152
O12w–H12b···O31 ^{vii}	0.99	1.91	2.8248(1)	153
O13w–H13A···O19 ^{viii}	1.00	2.08	2.9540(1)	145
O14w–H14A···O13 ^{xiv}	0.88	2.06	2.8709(1)	153
O14w–H14b···O3w ^{vi}	0.99	2.11	2.8026(1)	125
O15w–H15A···O10w ^{vi}	1.00	2.19	2.8638(1)	123
O15w–H15b···O8 ^{xiv}	1.01	1.92	2.7256(1)	134
O17w–H17A···O29 ^{vi}	0.99	1.96	2.8367(1)	145

^aD = donor, A = acceptor. ^bSymmetry code: (vi) x,y,z; (vii) = -1+x, y, z; (viii) = 2-x, 0.5+y, 1-z; (ix) = 1-x, -0.5+y, -z; (x) = 1-x, 0.5+y, -z; (xi) = 2-x, -0.5+y, 1-z; (xii) = 1-x, 0.5+y, -z; (xiii) = -1+x, y, 1+z; (xiv) = x, y, 1+z.

Table S14 – Hydrogen bonds in **2** (Å, deg)^{a,b}

	d(D–H)	d(H···A)	d(D···A)	<D···A
N3–H3N···O9 ^{xv}	0.860	2.082	2.883(6)	154.87
O2W–H3W···O8	0.850	1.890	2.677(6)	153.35
O2W–H4W···O5w	0.850	1.985	2.757(8)	150.27
N1–H1N···O3 ^{xvi}	0.860	2.147	2.980(7)	162.73
O5W–H8W···O6 ^{xvii}	0.993	2.009	2.754(8)	129.95
O3W–H5W···O5	0.850	1.980	2.794(7)	160.01
O1W–H2W···O2 ^{iv}	0.850	2.071	2.723(7)	133.10
O1W–H2W···O2w	0.850	2.443	2.940(8)	118.03
O4W–H7W···O3 ^{xvi}	0.993	2.259	3.126(15)	145.17

^aD = donor, A = acceptor. ^bSymmetry code: (xv) = 1.75-x, y, 0.75-z; (xvi) = x, 0.25-y, 0.25-z; (xvii) = 0.25-x, 0.25+y, 0.5-z.

Table S15 – Bond distances (Å) for the O_{oxamate}—Co—O_{oxamate} system in **3**^a

Co1–O8	2.024(13)
Co1–O1	2.073(13)
Co1–O7	2.078(13)
Co1–O2	2.098(12)
Co1–O2W	2.143(11)
Co1–O1W	2.151(11)
Co2–O11 ^{xviii}	1.979(14)
Co2–O4W	2.052(16)
Co2–O3W	2.103(15)
Co2–O10 ^{xviii}	2.108(15)
Co2–O4	2.107(15)
Co2–O5	2.110(13)

^aSymmetry code: (xviii) = $x-1, y+2, z+1$.Table S16 – Bond angles (deg) for the O_{oxamate}—Co—O_{oxamate} system in **3**^a

O8–Co1–O1	101.0(5)
O8–Co1–O7	79.6(5)
O1–Co1–O7	179.1(6)
O8–Co1–O2	178.0(7)
O1–Co1–O2	80.4(5)
O7–Co1–O2	99.0(5)
O8–Co1–O2W	88.2(4)
O1–Co1–O2W	88.0(5)
O7–Co1–O2W	92.8(5)
O2–Co1–O2W	93.3(4)
O8–Co1–O1W	90.4(5)
O1–Co1–O1W	90.8(5)
O7–Co1–O1W	88.5(5)
O2–Co1–O1W	88.1(4)
O2W–Co1–O1W	177.9(6)
O11 ^{xviii} –Co2–O4W	91.2(6)
O11 ^{xviii} –Co2–O3W	87.5(6)
O4W–Co2–O3W	178.4(8)
O11 ^{xviii} –Co2–O10 ^{xviii}	80.1(6)
O4W–Co2–O10 ^{xviii}	87.2(7)
O3W–Co2–O10 ^{xviii}	91.7(6)
O11 ^{xviii} –Co2–O4	101.0(6)
O4W–Co2–O4	91.1(7)
O3W–Co2–O4	90.0(6)
O10 ^{xviii} –Co2–O4	178.0(8)
O11 ^{xviii} –Co2–O5	178.3(7)
O4W–Co2–O5	90.3(6)
O3W–Co2–O5	91.0(5)
O10 ^{xviii} –Co2–O5	99.1(5)
O4–Co2–O5	79.8(5)

^aSymmetry code: (xviii) = $x-1, y+2, z+1$.

Table S17 – Bond distances (Å) for the O_{oxamate}—Co—O_{oxamate} system in **4**

Co1–O1W ^{xix}	2.079(2)
Co1–O1W	2.079(2)
Co1–O1 ^{xix}	2.086(2)
Co1–O1	2.086(2)
Co1–O2 ^{xix}	2.094(2)
Co1–O2	2.094(2)
Co2–O7 ^{xix}	2.088(2)
Co2–O7	2.088(2)
Co2–O4 ^{xx}	2.095(2)
Co2–O4	2.095(2)
Co2–O5 ^{xx}	2.096(2)
Co2–O5	2.096(2)

^aSymmetry code: (xix) = -*x*, -*y*+1, -*z*+1; (xx) = -*x*+1, -*y*+1, -*z*+1.

Table S18 – Bond angles (deg) for the O_{oxamate}—Co—O_{oxamate} system in **4**^a

O1W ^{xxi} –Co1–O1W	180.00(8)
O1W ^{xxi} –Co1–O1 ^{xxi}	92.91(9)
O1W–Co1–O1 ^{xxi}	87.09(9)
O1W ^{xxi} –Co1–O1	87.09(9)
O1W–Co1–O1	92.91(9)
O1 ^{xxi} –Co1–O1	180.0
O1W ^{xxi} –Co1–O2 ^{xxi}	89.65(9)
O1W–Co1–O2 ^{xxi}	90.36(9)
O1 ^{xxi} –Co1–O2 ^{xxi}	77.89(8)
O1–Co1–O2 ^{xxi}	102.10(8)
O1W ^{xxi} –Co1–O2	90.35(9)
O1W–Co1–O2	89.65(9)
O1 ^{xxi} –Co1–O2	102.11(8)
O1–Co1–O2	77.90(8)
O2 ^{xxi} –Co1–O2	180.0
O7 ^{xxii} –Co2–O7	180.0
O7 ^{xxii} –Co2–O4 ^{xxii}	88.09(10)
O7–Co2–O4 ^{xxii}	91.91(10)
O7 ^{xxii} –Co2–O4	91.91(10)
O7–Co2–O4	88.10(10)
O4 ^{xxii} –Co2–O4	180.0
O7 ^{xxii} –Co2–O5 ^{xxii}	90.62(9)
O7–Co2–O5 ^{xxii}	89.38(9)
O4 ^{xxii} –Co2–O5 ^{xxii}	78.74(8)
O4–Co2–O5 ^{xxii}	101.26(8)
O7 ^{xxii} –Co2–O5	89.39(9)
O7–Co2–O5	90.61(9)
O4 ^{xxii} –Co2–O5	101.26(8)
O4–Co2–O5	78.74(8)
O5 ^{xxii} –Co2–O5	180.0

^aSymmetry code: (xxi) = -*x*, -*y*+1, -*z*+1; (xxii) = -*x*+1, -*y*+1, -*z*+1.

Table S19 – Hydrogen bonds in **3** (Å, deg)^{a,b}

	d(D–H)	d(H···A)	d(D···A)	<D···A
N2–H2N···O1W ^{xxiii}	0.860	2.193	2.988	153.67
N2–H2N···O6	0.860	2.266	2.692	110.66
N1–H1N···O6W ^{xxiv}	0.860	2.409	3.240	162.63
N4–H4N···O2W ^{xxv}	0.860	2.218	3.032	158.10
O2W–H2WA···O12 ^{xxii}	0.857	2.577	3.055	116.31
O2W–H2WA···O6 ^{xxvi}	0.857	2.008	2.747	143.94
O2W–H2WB···O7W ^{xxiii}	0.860	2.115	2.761	131.52
O1W–H1WB···O12 ^{xxvii}	0.852	1.900	2.733	165.18
O1W–H1WB···O6 ^{xxv}	0.852	2.474	2.923	113.75
O1W–H1WA···O6W ^{xxviii}	0.851	2.364	3.152	154.14
O4W–H4WA···O3 ^{xxix}	0.883	1.828	2.686	163.45
O4W–H4WB···O8W ^{xxx}	0.844	2.161	2.958	157.51
O3W–H3WA···O9 ^{xxvii}	1.001	1.785	2.779	171.55
O3W–H3WB···O5W ^{xxvii}	0.855	1.928	2.705	150.34
O5W–H5WA···O2 ^{xxxii}	0.829	2.012	2.830	168.92
O5W–H5WB···O4 ^{xxv}	1.063	2.531	3.540	158.13
O5W–H5WB···O4W ^{xxv}	1.063	2.611	3.367	127.70
O7W–H7WB···O5 ^{xxxii}	0.890	1.879	2.618	139.12
O8W–H8WA···O8 ^{xxv}	0.994	2.129	2.867	129.55
O8W–H8WB···O10 ^{xxxii}	0.917	2.583	3.488	168.98
O6W–H6WB···O7 ^{xxxii}	0.993	2.508	3.128	120.22

^aD = donor and A = acceptor. ^bSymmetry code: (xxiii) = $x, y+1, z$; (xxiv) = $x, y+1, z-1$; (xxv) = $x, y-1, z$; (xxvi) = $x+1, y-1, z$; (xxvii) = $x-1, y+1, z$; (xxviii) = $x, y, z-1$; (xxix) = $x, y+1, z+1$; (xxx) = $x, y+2, z$; (xxxii) = $x, y, z+1$; (xxxiii) = $x+1, y-1, z$.

Table S20 – Hydrogen bonds in **4** (Å, deg)^{a,b}

	d(D–H)	d(H···A)	d(D···A)	<D···A
O7–H10···O2 ^{xxxiii}	0.860	2.193	2.988	153.67
O1w–H2w···N3	0.860	2.266	2.692	110.66
N1–H1N···N4 ^{xxxiv}	0.860	2.409	3.240	162.63
N2–H2N···O6 ^{xxxv}	0.860	2.218	3.032	158.10
O2W–H2WA···O12 ^{xxvii}	0.857	2.577	3.055	116.31
O2W–H3W···O3 ^{xxxiii}	0.857	2.008	2.747	143.94
O2W–H4W···N2 ^{xxxvii}	0.860	2.115	2.761	131.52

^aD = donor and A = acceptor. ^bSymmetry code: (xxxiii) = $-x, -y+1, -z+1$; (xxxiv) = $x-1, y, z$; (xxxv) = $-x, y+1/2, -z+1/2$; (xxxvi) = $-x+1, -y+1, -z$; (xxxvii) = $-x+1, -y+1, -z+1$.

Table S21 – Selected magneto-structural data of tetrahedral cobalt(II) complexes $[\text{Co}(\text{AA})\text{X}_2]$ (AA = didentate N -donor and X = halide)^{a,b}

Compound	CoN_2X_2	$\text{Co-N}/\text{\AA}$	$\text{Co-X}/\text{\AA}$	$\varphi_{\text{X}}/^\circ$	$\varphi_{\text{N}}/^\circ$	D/cm^{-1}	E/cm^{-1}	Ref
Pre-I	{CoN ₂ Cl ₂ }	2.062 2.028	2.234 2.250	118.46	117.73	+6.7	+0.98	This work
[Co(dmphen)Br ₂]	{CoN ₂ Br ₂ }	1.960 2.021	2.344 2.370	115.59	84.5	+10.62	-0.011	2
[Co(bcp)Cl ₂]	{CoN ₂ Cl ₂ }	2.037	2.211	119.99	81.64	-5.62	---	3
[Co(bcp)Br ₂]	{CoN ₂ Br ₂ }	2.039	2.331	120.77	81.86	-6.62	---	3
[Co(bcp)I ₂]	{CoN ₂ I ₂ }	2.030	2.524	121.69	82.13	-6.72	---	3
[Co(biq)Cl ₂]	{CoN ₂ Cl ₂ }	2.034	2.223	117.37	81.70	+10.5	0	4
[Co(biq)Br ₂]	{CoN ₂ Br ₂ }	2.033	2.256	117.86	81.90	+12.5	0	4
[Co(biq)I ₂]	{CoN ₂ I ₂ }	2.031	2.538	118.29	83.13	+10.3	4.1	4

^aAbbreviations of the ligands: dmphen = 2,9-dimethyl-1,10-phenanthroline), bcp = bathocuproine = 4,7-diphenyl-2,9-dimethyl-1,10-phenanthroline and biq = 2,2'-biquinoline.

^b φ_{X} and φ_{N} represent the X-Co-X and N-Co-N bond angles, respectively.

Table S23 – Cole-Cole parameters obtained and used to reproduce the Argand plots of 3

T/K	$\chi_{\text{T}}/\text{cm}^3 \text{mol}^{-1}$	$\chi_1/\text{cm}^3 \text{mol}^{-1}$	$\tau_1 \times 10^4/\text{s}$	α_1	$\chi_2/\text{cm}^3 \text{mol}^{-1}$	$\tau_2 \times 10^5/\text{s}$	α_2
2.75	0.13	0.23	11.2	0.22	0.19	4.09	0.26
3.00	0.13	0.23	9.41	0.25	0.16	3.26	0.23
3.25	0.12	0.20	8.54	0.22	0.16	3.06	0.27
3.50	0.10	0.17	7.63	0.18	0.17	2.85	0.31
3.75	0.10	0.16	6.93	0.17	0.16	2.69	0.33
4.00	0.09	0.15	6.08	0.17	0.15	2.43	0.33
4.25	0.09	0.14	5.38	0.16	0.14	2.28	0.33
4.50	0.09	0.14	4.69	0.17	0.13	1.94	0.32
4.75	0.08	0.14	4.11	0.19	0.12	1.69	0.33
5.00	0.08	0.13	3.68	0.17	0.11	1.67	0.31
5.50	0.08	0.12	3.00	0.16	0.09	1.65	0.31
6.00	0.08	0.11	2.41	0.15	0.08	1.59	0.28
6.50	0.08	0.08	1.99	0.09	0.10	2.50	0.30
7.00	0.08	0.08	1.53	0.08	0.06	1.86	0.20
7.50	0.08	0.08	1.03	0.05	0.06	1.58	0.16
8.00	0.07	0.06	0.645	0.00	0.08	1.48	0.24

Table S24 – Cole-Cole parameters obtained and used to reproduce the Argand plots for **4**

T / K	$\chi_{\text{S}} / \text{cm}^3 \text{ mol}^{-1}$	$\chi_{\text{S}} / \text{cm}^3 \text{ mol}^{-1}$	$\tau_1 \times 10^5 / \text{s}$	A
4.0	0.34	0.46	4.38	0.17
4.5	0.31	0.42	3.81	0.15
5.0	0.28	0.39	3.24	0.13
5.5	0.26	0.36	2.71	0.11
6.0	0.24	0.33	2.27	0.09
6.5	0.23	0.31	1.75	0.09
7.0	0.21	0.29	1.39	0.08

Table S22- Selected dc magnetic of six-coordinate octahedral cobalt(II) complexes*

Compound	σ / cm^{-1}	λ / cm^{-1}	ν / cm^{-1}	$\Delta_{\text{ax}}^{(\text{d})}$	Δ_{rh}	u / cm^{-1}	g_{eff}	D / cm^{-1}	E / cm^{-1}	zJ / cm^{-1}	Ref
1 (Co1-Co4)	-0.8	-145	-172.4	-331.0		-				-	This work
(Co5-Co6)	-1.5	-180	-84.6 ^(a)	-571.1		-				-	
2 (Co1/Co2)							2.6/2.2	22.3/22.3	2.1/1.0	-0.02	This work
3	-0.98	-180	-145	-417.8		3.8 ^(b)				-0.11	This work
4 (Co1/Co2)							2.57	54	2.8	-0.02	This work
<i>cis</i> -[Co(hfac) ₂ (H ₂ O) ₂]	1.34 ^(c)	-147.2		-499.7	136.3						5
[Co(dca) ₂ (bim) ₄]	-1.18 ^(c)	-132.0		-416.3							6
[Co(dca) ₂ (bim) ₂] _n	-1.16 ^(c)	-134.1		-402.7							6
[Co(dca) ₂ (bmim) ₂] _n	-1.24 ^(c)	-134.0		-605.8							6
[Co(dca) ₂ (atz) ₂] _n	-1.18(1) ^(c)	-125(1)		-509(10)							7
[Co(ppad) ₂] _n	-1.48(1) ^(c)	-147(1)		-428(5)			2.46	76	6.5		8
[Co(CH ₃ COO) ₂ (py) ₂ (H ₂ O) ₂]	-1.5 ^(c)	-170		-279	109						9
[Co(pydm) ₂](dnbz) ₂	-0.61 ^(c)	-187		-585							10
[Co(CH ₃ COO) ₂ (H ₂ O) ₂ (MeIm) ₂]	-1.38 ^(c)	-171.7		503							11
TBA ₂ [Co ₂ (H ₂ mpba) ₃]·2dmf·5H ₂ O	0.99	-128		-391							12
(HNEt ₃) ₂ [Co ₂ (H ₂ mpba) ₃]·6dmf·5H ₂ O	0.76	-179		-565							12
(HNEt ₃) ₂ [Co ₂ (H ₂ mpba) ₃]	0.79	-168		-494							12
<i>cis</i> -[Co(dmphen) ₂ (NCS) ₂]·0.25EtOH	1.225 ^(c)	-165.8		493	22.5		2.78	98	8.4		13
<i>trans</i> -[Co(acac) ₂ (H ₂ O) ₂]							2.5	57	18		14
<i>trans</i> -[Co(abpt) ₂ (tcm) ₂]							2.46	48	13		15
[Co(μ -L ¹)(μ -CH ₃ COO)Y(NO ₃) ₂]	1.421 ^(c)	-109.2		645.5	-55.8		2.503	42	2		16
[Co(bzpy) ₄ Cl ₂]							2.527	106			17
[Co(bzpy) ₄ (NCS) ₂]							2.525	90			17
[Co(dpmm ^{0,0}) ₃][CoBr ₄]							2.2	147			18
							2.41	12.3			
α -[Co(3,5-Hdnb) ₂ (py) ₂ (H ₂ O) ₂]							2.7	58	0.1		19
β -[Co(3,5-Hdnb) ₂ (py) ₂ (H ₂ O) ₂]							2.42	68	15		19

*Abbreviations of the ligands: hfac = hexafluoroacetylacetone, dca = dicyanamide, bim = 1-benzylimidazole, bmim = 1-benzyl-2-methylimidazole, atz = 2-amino-1,3,5-triazine, ppad = N^3 -(3-pyridoyl)-3-pyridinecarboxamidrazone, pydm = 2,6-pridinedimethanol, dnbz = 3,5-dinitrobenzoato(1-), MeIm = 1-methylimidazole,

Et ₄ N[Co(hfac) ₃]	-1.11 ^(c)	-180	428.29	90.34	2.48	118	10	19
[Co ^{III} Co ^{II} (H ₂ L ²) ₂ (Cl)(H ₂ O)](H ₂ O) ₄	-1.40	-89	339					20
[Co ^{III} Co ^{II} (H ₂ L ²) ₂ (Br)(H ₂ O)](H ₂ O) ₄	-1.36	-114	-560					20
[Co ^{III} Co ^{II} (H ₂ L ²) ₂ (NO ₃)(H ₂ O)](H ₂ O) ₃	-1.43	-113	547					20
[Co ^{II} Co ^{III} (H ₂ L ²) ₂ (CH ₃ COO)(H ₂ O)]	-1.49	-176	-711	44				21
[Co ^{II} ₂ Co ^{III} ₂ (L ³) ₄ (CH ₃ COO) ₂ (MeOH) ₂]·Et ₂ O	-1.18	-57	351					22
{[Co ^{III} (L ⁴) ₂][Co ^{II} (bpy) ₂]ClO ₄ ·H ₂ O} _∞	-1.27	-162	488					23
{[Co ^{III} (L ⁴) ₂][Co ^{II} (phen) ₂]ClO ₄ ·H ₂ O} _∞	-1.23	-165	472					23
{[Co ^{III} (L ⁵) ₂][Co ^{II} (bpy)(MeOH) ₂]ClO ₄ ·H ₂ O} _∞	-1.21	-172	473					23
[{Co(μ -L ⁶)Y(NO ₃) ₂ } ₂ (μ -CO ₃) ₂]·2MeOH·2H ₂ O	-1.5	-105	-661					24

H₄mpba = 1,3-phenylenebis(oxamic acid), dmphen = 2,9-dimethyl-1,10-phenanthroline, acac = acetylacetone; bpt = 4-amino-3,5-bis(2-pyridyl)-1,2,4-triazole, tcm = tricyanomethane anion; H₂L¹ = N,N',N''-trimethyl-N,N''-bis(2-hydroxy-3-methoxy-5-methylbenzyl)-diethylenetriamine, bzpy = 4-benzylpyridine, dppm^{0,0} = bis(diphenylphosphanoxido)methane, 3,5-Hdnb = 3,5-dinitrobenzoic acid; py = pyridine; H₄L² = 2-[{(2-hydroxy-3-methoxyphenyl)methylene}amino]-2-(hydroxymethyl)-1,3-propane-diol, H₂L³ = 2-oxo-quinoline-3-carbaldehyde; H₂L⁴ = N-salicylidene-L-alanine, H₂L⁵ = N-salicylidene-L-phenylalanine, bpy = 2,2'-bipyridine ; phen = 1,10-phenanthroline and H₂L⁶ = N,N',N''-trimethyl-N,N''-bis(2-hydroxy-3-methoxy-5-methylbenzyl)diethylenetriamine).

^(a)Co5 = Co6.

^(b)Co1 and Co2.

^(c)Calculated values taking into consideration the Griffith-Figgis Hamiltonian.

^(d) $\Delta_{ax} = 3\sigma^2\nu$.

Table S25- Selected ac magnetic data of six-coordinate octahedral cobalt(II) complexes

Compound	τ_0 / s	B_{DC} / T	$U_{\text{eff}} / \text{cm}^{-1}$	$A / \text{s}^{-1} \text{K}^{-1}$	$B / \text{s}^{-1} \text{K}^{-n}$	$C / \text{s}^{-1} \text{K}^{-n}$	m	n	Effect	Observ.	Ref
1	--	--	--	--	--	--	--	--	--	Easy axis Anisotropy	This work
2	--	--	--	--	--	--	--	--	--	Easy plane anisotropy	This work
3	$1.3(0.1) \times 10^{-10}^{(\text{a})}$		$110(10)^{(\text{a})}$		$105(1)^{(\text{a})}$		$2.0(1)^{(\text{a})}$		Orbach	Easy axis Anisotropy	This work
					$54(9) \times 10^2^{(\text{b})}$			$1.5(0.1)^{(\text{b})}$		Bottleneck	
4				$61(2) \times 10^2$		$0.4(4)$		$6.0(6)$	Direct	Easy plane anisotropy	This work
<i>cis</i> -[Co(hfac) ₂ (H ₂ O) ₂]		0.1		7225.7		106.4		4.9	Raman Direct	Easy axes anisotropy	5
[Co(dca) ₂ (bim) ₄]	0.87×10^{-6}	0.25	7.74						Raman Orbach	Easy axes anisotropy	6
[Co(dca) ₂ (bim) ₂] _n	1.54×10^{-6}	0.25	5.33						Orbach	Easy axes anisotropy	6
[Co(dca) ₂ (bmim) ₂] _n	0.63×10^{-6}	0.25	13.81						Orbach	Easy axes anisotropy	6
[Co(dca) ₂ (atz) ₂] _n	1.7×10^{-6}	0.1	5.1						Orbach	Easy axes anisotropy	7
[Co(ppad) ₂] _n	5.03×10^{-6}	0.2	11.37						Orbach	Easy axes anisotropy	8
[Co(CH ₃ COO) ₂ (C ₂ H ₅ N) ₂ (H ₂ O) ₂] ^(c)	6.7×10^{-7}	0.15	25.0						Orbach	Easy axes anisotropy	9
[Co(pydm) ₂](dnbz) ₂	$2.8(4) \times 10^{-9}^{(\text{a})}$	0.2	$44.1(8)^{(\text{a})}$			$72(28)^{(\text{a})}$		$2.3^{(\text{a})}$	Tunneling Raman	Easy axes anisotropy	10
[Co(bzpy) ₄ Cl ₂] ^(d)		0.4				4.16		5	Orbach Raman Tunneling	Easy plane anisotropy	17
[Co(bzpy) ₄ (NCS) ₂]	1.2×10^{-6}	0.2	22.9		1.19×10^4		2		Bottleneck Orbach	Easy plane anisotropy	17
α -[Co(3,5-Hdnb) ₂ (py) ₂ (H ₂ O) ₂]		0.1		14(10)		0.64(5)		6.45(4)	Direct Raman	Easy plane anisotropy	19

β -[Co(3,5-Hdnb) ₂ (py) ₂ (H ₂ O) ₂]		0.1		139(44)		0.28(4)	7.07(7)	Direct Raman	Easy plane anisotropy	19
Et ₄ N[Co(hfac) ₃]	6.4(9) x 10 ⁻⁶ ^(a) 9(5) x 10 ⁻⁶ ^(b)	0.1	20.6(5) ^(a) 18(2) ^(b)	96.3 ^(a) 1420 ^(b)		2.2(2)	6	Direct Raman Orbach	Easy plane anisotropy	20
[Co ^{III} Co ^{II} (H ₂ L ²) ₂ (Cl)(H ₂ O)] · 4H ₂ O	6.1 x 10 ⁻⁶	0.1	7.1					Orbach	Easy plane anisotropy	21
[Co ^{III} Co ^{II} (H ₂ L ²) ₂ (Br)(H ₂ O)] · 4H ₂ O	1.0 x 10 ⁻⁶	0.1	14.5					Orbach	Easy axes anisotropy	21
[Co ^{III} Co ^{II} (H ₂ L ²) ₂ (NO ₃)(H ₂ O)] · 3H ₂ O									Easy plane anisotropy	21
[Co ^{II} Co ^{III} (H ₂ L ²) ₂ (CH ₃ COO)(H ₂ O)]	7.1(9) x 10 ⁻⁶ ^(b) 3.2(7) x 10 ⁻⁶ ^(b) 0.54(49) x 10 ⁻⁶ ^(b)	0.1 ^(b) 0.2 ^(b) 0.4 ^(b)	16.1(7) ^(b) 18.0(10) ^(b)	100(20) ^(b) 368(32) ^(b) 366.08(23) ^(b)				Direct Orbach	Easy axes anisotropy	22
				24.4(39) ^(b)						
[Co ^{II} ₂ Co ^{III} ₂ (L ³) ₄ (CH ₃ COO) ₂ (MeOH) ₂] · Et ₂ O	5.5 x 10 ⁻⁸	0.1	68.8		2.6(3)		6.7(3)	Raman Orbach	Easy plane anisotropy	23
[{Co(μ -L ⁶)Y(NO ₃) ₂ (μ -CO ₃) ₂ } · 2MeOH · 2H ₂ O		0.025 0.2			0.00014 0.005		1.16 2.18	Raman	Easy axes anisotropy	25

Hfac = hexafluoroacetylacetone, dca = dicyanamide, bim = 1-benzylimidazole, bmim = 1-benzyl-2-methylimidazole, atz = 2-amino-1,3,5-triazine, ppad= *N*³-(3-pyridoyl)-3-pyridinecarboxamidrazone, pydm = 2,6-pyridinedimethanol, dnbz = 3,5-dinitrobenzoato(1-), MeIm = 1-methylimidazole, bpt = 4-amino-3,5-bis(2-pyridyl)-1,2,4-triazole, tcm = tricyanomethane anion, bzpy = 4-benzylpyridine, 3,5-Hdnb = 3,5-dinitrobenzoic acid, py = piridine, H₄L² = 2-[{(2-hydroxy-3-methoxyphenyl)methylene}amino]-2-(hydroxymethyl)-1,3-propane-diol, H₂L³ = 2-oxo-quinoline-3-carbaldehyd and H₂L⁶ = *N,N,N',N'*-trimethyl-*N,N'*-bis(2-hydroxy-3-methoxy-5-methylbenzyl)diethylenetriamine).

^(a) Low frequency, ^(b) High frequency.

^(c) τ_{QTM} = 0.011 s.

^(d) τ_{QTM} = 2.63 x10⁻⁴ s.

References

- 1 O. Scarlat and M. Zaharescu, *J. Therm. Anal. Calorim.*, 2002, **68**, 851.
- 2 S. Vaidya, A. Upadhyay, S. K. Singh, T. Gupta, S. Tewary, S. K. Langley, J. P. S. Walsh, K. S. Murray, G. Rajaraman and M. Shanmugam, Synthetic strategy for switching the single ion anisotropy in tetrahedral Co(II) complexes. *Chem. Commun.*, 2015, **51**, 3739.
- 3 J. Titiš, J. Miklovič and R. Boča, Magnetostructural study of tetracoordinate cobalt(II) complexes. *Inorg. Chem. Commun.*, 2013, **35**, 72.
- 4 M. Idešicová, L. Dlháň, J. Moncoľ, J. Titiš and R. Boča, Zero-field splitting in tetracoordinate Co(II) complexes. *Polyhedron*, 2012, **36**, 79.
- 5 D. V. Korchagin, A. V. Palii, E. A. Yureva, A. V. Akimov, E. Y. Misochko, G. V. Shilov, A. D. Talantsev, R. B. Morgunov, A. A. Shakin, S. M. Aldoshin and B. S. Tsukerblat, Evidence of field-induced slow magnetic relaxation in cis-[Co(hfac)₂(H₂O)₂] exhibiting tri-axial anisotropy with a negative axial component. *Dalton Trans.*, 2017, **46**(23), 7540-.
- 6 A. Świtlicka-Olszewska, J. Palion-Gazda, B. Macura, J. Cano, F. Lloret and J. Cano, Single-ion magnet behavior in mononuclear and two-dimensional dicyanamide-containing cobalt(II) complexes. *Dalton Trans.*, 2016, **45**, 10181.
- 7 J. Palion-Gazda, T. Klemens, B. Machura, J. Vallejo, F. Lloret and M. Julve, Single ion magnet behaviour in a two-dimensional network of dicyanamide-bridged cobalt (II) ions. *Dalton Trans.*, 2015, **44**(7), 2989..
- 8 X. Liu, L. Sun, H. Zhou, P. Cen, X. Jin, G. Xie, S. Chen and Q. Hu, Single-Ion-Magnet Behavior in a Two-dimensional coordination polymer constructed from CoII nodes and a pyridylhydrazone derivative. *Inorg. chem.*, 2015, **54**(18), 8884.

- 9 J. P. Walsh, G. Bowling, A. M. Ariciu, N. F. Jailani, N. F. Chilton, P. G. Waddell, D. Collison, F. Tuna and L. J. Higham, Evidence of slow magnetic relaxation in $\text{Co}(\text{AcO})_2(\text{py})_2(\text{H}_2\text{O})_2$. *Magnetochemistry*, 2016, **2**(2), 23.
- 10 D. Valigura, C. Rajnák, J. Moncol, J. Titiš and R. Boča, A mononuclear Co(II) complex formed from pyridinedimethanol with manifold slow relaxation channels. *Dalton Trans.*, 2017, **46**(33), 10950.
- 11 B. Papánková, R. Boča, L. Dlháň, I. Nemec, J. Titiš, I. Svoboda and H. Fuess, Magneto-structural relationships for a mononuclear Co(II) complex with large zero-field splitting. *Inorg. Chim. Acta*, 2010, **363**(1), 147.
- 12 L. Lisnard, L. M. Chamoreau, Y. Li and Y. Journaux, Solvothermal Synthesis of Oxamate-Based helicates: Temperature Dependence of the Hydrogen Bond Structuring in the Solid. *Cryst. Growth Des.*, 2012, **12**, 4955.
- 13 J. Vallejo, I. Castro, R. Ruiz-García, J. Cano, M. Julve, F. Lloret, G. De Munno, W. Wernsdorfer and E. Pardo, Field-induced slow magnetic relaxation in a six-coordinate mononuclear cobalt (II) complex with a positive anisotropy. *J. Am. Chem. Soc.*, 2012, **134**(38), 15704.
- 14 S. Gómez-Coca, A. Urtizberea, E. Cremades, P. J. Alonso, A. Camón, E. Ruiz and F. Luis, Origin of slow magnetic relaxation in Kramers ions with non-uniaxial anisotropy. *Nat. Commun.*, 2014, **5**(1), 1.
- 15 R. Herchel, L. Váhovská, I. Potočnák and Z. Trávníček, Slow magnetic relaxation in octahedral cobalt (II) field-induced single-ion magnet with positive axial and large rhombic anisotropy. *Inorg. Chem.*, 2014, **53**(12), 5896.
- 16 E. Colacio, J. Ruiz, E. Ruiz, E. Cremades, J. Krzystek, S. Carretta, J. Cano, T. Guidi, W. Wernsdorfer and E. K. Brechin, Slow Magnetic Relaxation in a $\text{Co}^{\text{II}}\text{--Y}^{\text{III}}$

Single-Ion Magnet with Positive Axial Zero-Field Splitting. *Angew. Chem., Int. Ed.*, 2013, **52**, 9130.

17 C. Rajnák, J. Titiš, J. Moncoľ, F. Renz and R. Boča, Field-Supported Slow Magnetic Relaxation in Hexacoordinate CoII Complexes with Easy Plane Anisotropy. *Eur. J. Inorg. Chem.*, 2017, **11**, 1520.

18 F. Varga, C. Rajnak, J. Titiš, J. Moncoľ and R. Boča., Slow magnetic relaxation in a Co(II) octahedral–tetrahedral system formed of a $[CoL_3]^{2+}$ core with L=bis(diphenylphosphanoxydo) methane and tetrahedral $[CoBr_4]^{2-}$ counter anions. *Dalton Trans.*, 2017, **46**(13), 4148.

19 S. Roy, I. Oyarzabal, J. Vallejo, J. Cano, E. Colacio, A. Bauza, A. Frontera, A. M. Kirillov, M. G. B. Drew and S. Das, Two Polymorphic Forms of a Six-Coordinate Mononuclear Cobalt (II) Complex with Easy-Plane Anisotropy: Structural Features, Theoretical Calculations, and Field-Induced Slow Relaxation of the Magnetization. *Inorg. Chem.*, 2016, **55**(17), 8502.

20 A. V. Palii, D. V. Korchagin, E. A. Yureva, A. V. Akimov, E. Y. Misochko, G. V. Shilov, A. D. Talantsev, R. B. Morgunov, S. M. Aldoshin and B. S. Tsukerblat, Single-ion magnet $Et_4N[Co^{II}(hfac)_3]$ with non-uniaxial Anisotropy: Synthesis, experimental characterization, and theoretical modeling. *Inorg. Chem.*, 2016, **55**, 9696.

21 V. Chandrasekhar, A. Dey, A. J. Mota and E. Colacio, Slow magnetic relaxation in Co(III)–Co(II) mixed-valence dinuclear complexes with a $Co^{II}O_5X$ ($X= Cl, Br, NO_3$) distorted-octahedral coordination sphere. *Inorg. Chem.*, 2013, **52**, 4554.

22 E. A. Buvaylo, E.A.; V. N. Kokozay, V.N.; O. Y. Vassilyeva, O.Y.; B. W. Skelton, B.W.; A. Ozarowski, J. Titiš, B. Vranovičová and R. Boča, Field-Assisted Slow Magnetic Relaxation in a Six-Coordinate Co(II)–Co(III) Complex with Large Negative Anisotropy. *Inorg. Chem.*, 2017, **56**, 6999.

- 23 W. Huang, F. Pan, Z. Wang, Y. Bai, X. Feng, J. Gu, Z. W. Ouyang and D. A. Wu, mixed-valence metallogrid $[\text{Co}^{\text{III}}_2 \text{Co}^{\text{II}}_2]$ with an unusual electronic structure and single-ion-magnet characterization. *Dalton Trans.*, 2017, **46**, 5069.
- 24 S. Ganguly, P. Kar, M. Chakraborty, K. Sarkar and A. Ghosh, Synthesis, structure and phenoxazinone synthase-like activity of three unprecedented alternating $\text{Co}^{\text{II}}\text{--Co}^{\text{III}}$ 1D chains. *New J. Chem.*, 2019, **43**, 18780.
- 25 A. Masegosa, M. A. Palacios, E. Ruiz, S. Gómez-Coca, J. Krzystek, J. M. Moreno and E. Colacio, Dinuclear $\text{Co}^{\text{II}}\text{Y}^{\text{III}}$ vs. tetranuclear $\text{Co}^{\text{II}}_2\text{Y}^{\text{III}}_2$ complexes: the effect of increasing molecular size on magnetic anisotropy and relaxation dynamics. *Dalton Trans.*, 2019, **48**, 14873.